Article

Structure

Structural interactions define assembly adapter function of a type II secretion system pseudopilin

Graphical abstract

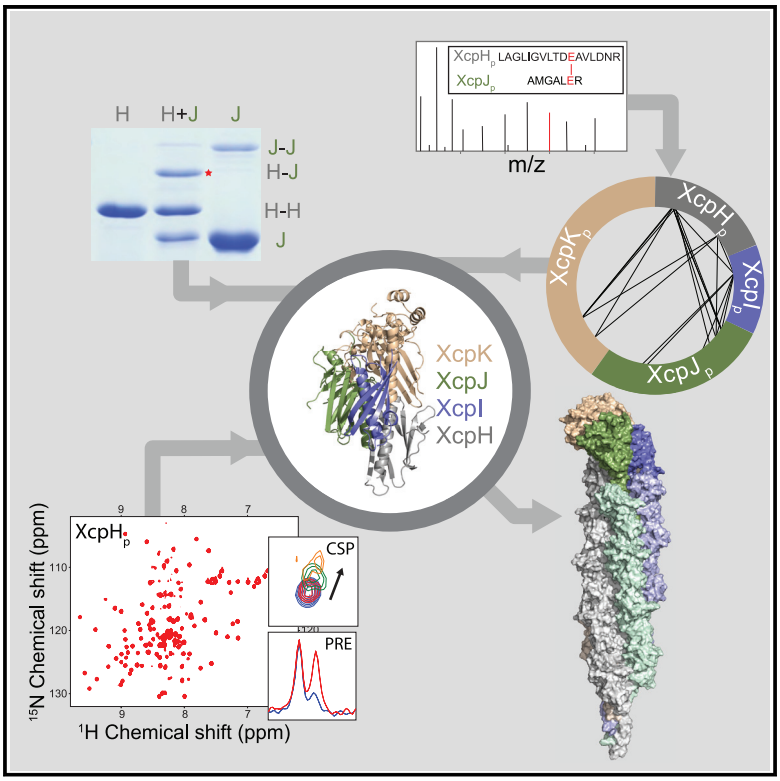

Highlights

- All four *P. aeruginosa* minor T2SS pseudopilins are essential for type II secretion
- GspH is integrated into the GspJIK tip complex through a defined GspH-J interface
- GspH adapts pseudopilus tip to body, requiring unraveling of the GspH α1N helix
- In the pseudopilus, each protofilament is capped by one of four minor pseudopilins

Authors

Cristian A. Escobar, Badreddine Douzi, Geneviève Ball, ..., Loïc Quinton, Romé Voulhoux, Katrina T. Forest

Correspondence

loic.quinton@uliege.be (L.Q.), voulhoux@imm.cnrs.fr (R.V.), forest@bact.wisc.edu (K.T.F.)

In brief

Escobar, Douzi, et al. apply NMR methods, cross-linking mass spectrometry, and computational modeling to describe the complete structure of the filament underlying the type II secretion system. The GspH subunit requires secondary structure remodeling to form the crucial link from the globular tip complex into the homopolymeric pilus.

Escobar et al., 2021, Structure *29*, 1–12
October 7, 2021
https://doi.org/10.1016/j.str.2021.05.015

CellPress

Please cite this article in press as: Escobar et al., Structural interactions define assembly adapter function of a type II secretion system pseudopilin, Structure (2021), https://doi.org/10.1016/j.str.2021.05.015

Structure

CellPress

Article

Structural interactions define assembly adapter function of a type II secretion system pseudopilin

Cristian A. Escobar,[1,4,7] Badreddine Douzi,[2,5,7] Geneviève Ball,[2] Brice Barbat,[2] Sebastien Alphonse,[2,6] Loïc Quinton,[3,*] Romé Voulhoux,[2,*] and Katrina T. Forest[1,8,*]

[1]Department of Bacteriology, University of Wisconsin-Madison, Madison, WI, USA
[2]Laboratoire de Chimie Bactérienne (UMR7283), Institut de Microbiologie de la Méditerranée, CNRS-Aix Marseille Université, Marseille, France
[3]Laboratory of Mass Spectrometry, MolSys Research Unit, University of Liège, Liège, Belgium
[4]Present address: Department of Biochemistry, University of Wisconsin-Madison, Madison, WI, USA
[5]Present address: Université de Lorraine, INRAE, DynAMic, F-54000 Nancy, France
[6]Present address: Department of Chemistry, CCNY, New York, NY, USA
[7]These authors contributed equally
[8]Lead contact
*Correspondence: loic.quinton@uliege.be (L.Q.), voulhoux@imm.cnrs.fr (R.V.), forest@bact.wisc.edu (K.T.F.)
https://doi.org/10.1016/j.str.2021.05.015

SUMMARY

The type IV filament superfamily comprises widespread membrane-associated polymers in prokaryotes. The type II secretion system (T2SS), a virulence pathway in many pathogens, belongs to this superfamily. A knowledge gap in understanding of the T2SS is the molecular role of a small "pseudopilin" protein. Using multiple biophysical techniques, we have deciphered how this missing component of the Xcp T2SS architecture is structurally integrated, and thereby unlocked its function. We demonstrate that low-abundance XcpH is the adapter that bridges a trimeric initiating tip complex, XcpIJK, with a periplasmic filament of XcpG subunits. Each pseudopilin protein caps an XcpG protofilament in an overall pseudopilus compatible with dimensions of the periplasm and the outer membrane-spanning secretin through which substrates pass. Unexpectedly, to fulfill its adapter function, the XcpH N-terminal helix must be unwound, a property shared with XcpG subunits. We provide an experimentally validated three-dimensional structural model of a complete type IV filament.

INTRODUCTION

Bacteria have sophisticated secretory nanomachines that evolved to deliver exoproteins to the bacterial cell surface, into the surrounding medium, or directly into host cells. Among these, the type II secretion system (T2SS) is a *trans*-envelope apparatus specialized for secretion of folded proteins from Gram-negative bacteria (Korotkov and Sandkvist, 2019). In many cases, these secreted substrates are virulence factors: examples include cholera toxin of *Vibrio cholerae*, exotoxin A of *Pseudomonas aeruginosa*, and heat-labile toxin of enterotoxigenic *Escherichia coli* (Cianciotto and White, 2017). The conformational constraint of transporting folded substrates is shared by the type VII, or ESX, system (Sysoeva et al., 2014) and the T9SS (Lasica et al., 2017), but is in clear contrast to the linear export of unfolded polypeptides by the T3SS (Evdokimov et al., 2003) or the T4SS (Trokter and Waksman, 2018). The substrates of the T2SS are not known to share any sequence or 3D structural motifs (Thomassin et al., 2017), and thus an open question is how substrates are individually recognized and ushered out. Dynamic and changing interactions, potentially involving nucleation of structure in intrinsically disordered regions, must be at the heart of this selection process (Gu et al., 2017).

The T2SS accomplishes its task with a distinctive mode of transport involving a pilus-like structure (the pseudopilus) in the periplasmic space, at the interface between an inner membrane assembly platform and a large outer membrane secretin (Hu et al., 2002). Structural, functional, and evolutionary commonalities to the extracellular type IV pili (T4Ps) critically inform the T2SS field and vice versa (Berry and Pelicic, 2015). Thanks to recent spectacular developments in cryoelectron microscopy, the 3D structures of T2SS secretins (Chernyatina and Low, 2019; Hay et al., 2017, 2018; Yan et al., 2017) and the filament formed upon overexpression of the pseudopilin subunit PulG (Lopez-Castilla et al., 2017) have been solved, and they reveal important features. While secretins form a tightly gated giant double β-barreled pore of 80 Å diameter in the outer

Please cite this article in press as: Escobar et al., Structural interactions define assembly adapter function of a type II secretion system pseudopilin, Structure (2021), https://doi.org/10.1016/j.str.2021.05.015

membrane, PulG adopts a right-handed homopolymeric helix with a 70 Å diameter, compatible with observations that a filament extends through the secretin when the pseudopilin is overexpressed (Durand et al., 2005; Vignon et al., 2003). In this pseudopilus, inter-subunit contacts occur along hydrophobic N-terminal α helices, with a special role for negatively charged glutamic acid at position 5 in both recruiting and stabilizing interactions (Craig et al., 2019; Nivaskumar et al., 2016; Parge et al., 1995; Pasloske et al., 1989). It has long been assumed that under native expression levels the pseudopilin forms a short and transient thread entirely within the periplasm during secretion (McLaughlin et al., 2012), a model that has been difficult to verify experimentally until recently, when a cryoelectron tomography reconstruction of the *Legionella pneumophil*a T2SS revealed pseudopilus density in ~20% of complexes, which was absent in mutant strains lacking pseudopilins (Ghosal et al., 2019).

In addition to the major pseudopilin, additional low-abundance (or minor) pseudopilins have been identified in the T2SS, based on being encoded within the same operon and sharing amino acid sequence with the pseudopilin, plus undergoing maturation by prepilin peptidase (Bally et al., 1992; Bleves et al., 1998; Nunn and Lory, 1993). The four minor pseudopilins are generally designated as H, I, J, and K proteins (variously prefixed with Gsp-, Pul-, or Xcp-, depending on the particular T2SS, see STAR Methods). While none of these has been directly observed in a T2SS pseudopilus, the periplasmic domains of minor pseudopilins GspI, GspJ, and GspK have the ability to assemble into a ternary complex whose crystal structure has been solved (Korotkov and Hol, 2008; Zhang et al., 2018). The four periplasmic domains of GspH, GspI, GspJ, and GspK form a quaternary complex (Douzi et al., 2009; Zhang et al., 2018), but its structure has been elusive. As a group, the minor pseudopilins are known to play a role in initiation and control of pseudopilus assembly and potentially retraction. The complex furthermore interacts with secretion substrates (Douzi et al., 2011) and with periplasmic domains of the secretin (Reichow et al., 2010). Korotkov and Hol (2008) proposed that if the GspIJK complex is associated with the GspG filament it can be positioned only at the tip of the pseudopilus and not at the base, in order to be compatible with the α-helical organization of GspG homomultimers. Regrettably, minor pseudopilin subunits could not be resolved in the *L. pneumophila* T2SS cryoelectron tomograms described above (Ghosal et al., 2019). However, cryoelectron tomography studies carried out on the closely related envelope-embedded T4P revealed a short stem-like structure in the periplasm that depends on expression of the minor pilins, which are analogous to the T2SS minor pseudopilins (Chang et al., 2016). More recently, a stub was shown to remain in subtomogram averages even in the absence of the major pilin and was thus proposed to be the priming complex of minor pilins (Treuner-Lange et al., 2020). Taken together these lines of evidence imply that minor pseudopilins form a short priming complex in the inner membrane, extending into the periplasm, under which the major pseudopilin subunits assemble. The molecular organization of this complex remains to be determined.

While many reports have established the importance of the minor pseudopilins and minor pilins as a group for initiation and/or assembly of (pseudo)pili, fewer have analyzed their individual contributions to secretion. Nonetheless, specific roles have been assigned or proposed for all four minor pseudopilins: GspJ primes filament assembly through the recruitment of other minor pseudopilins (Cisneros et al., 2012), GspI serves as a protein-protein interaction hub (Douzi et al., 2009), and GspK controls pseudopilus length and/or number (Cisneros et al., 2012; Douzi et al., 2009). GspH interacts with GspJ through its globular domain and with the structurally similar major pseudopilin via its N-terminal hydrophobic α helices (Nivaskumar et al., 2016; Douzi et al., 2009; Korotkov and Hol, 2008; Yanez et al., 2008a); thus, it is tempting to suggest GspH plays an adapter function between a pseudopilus tip complex and the body of the pseudopilus. However, the essentiality of GspH for secretion has been called into question because its absence can be overcome by overproduction of other minor pseudopilins (Cisneros et al., 2012). There are no molecular data on how GspH is embedded in the quaternary complex.

Based on X-ray crystallographic structures of periplasmic domains of GspH, GspI, GspJ, and GspK from several microbial species solved alone and/or in dimeric or trimeric subcomplexes (Zhang et al., 2018; Franz et al., 2011; Lam et al., 2009; Korotkov and Hol, 2008; Yanez et al., 2008a, 2008b), each pseudopilin fold resembles major T2SS pseudopilins and T4P major pilins characterized by an extended N-terminal α helix, the first half of which (α1N) is not included in the soluble crystallography targets but is expected to be exposed to the membrane environment, and the second half of which (α1C) is partially buried in a globular α/β domain. Despite this common overall topology, it is important to bear in mind that the periplasmic domains of the minor pseudopilins interact to form the soluble quaternary complex in the absence of α1N, and since these minor subunits are at the tip of the pseudopilus, they cannot depend on vertical interactions with major subunits for upward assembly. Within this general framework, each minor pseudopilin has hallmarks. GspH is most similar in size, sequence, and structure to the major pseudopilin. GspI is the smallest of the four. GspJ is larger, and displays a pronounced groove on its surface. Finally, GspK carries an additional structural domain of over 100 amino acids. GspH, GspI, and GspJ share the glutamate at position 5 with GspG, whereas GspK does not.

Based on two crystal structures of ternary complexes of minor pseudopilin periplasmic domains (PDB: 3CI0 from the enterotoxigenic *E. coli* Gsp T2SS, and PDB: 5VTM from the *P. aeruginosa* Xcp T2SS equivalent minor pilins XcpIJK [Korotkov and Hol, 2008; Zhang et al., 2018]), we know stabilizing interactions among the periplasmic domains $GspI_p$, $GspJ_p$, and $GspK_p$ include buried salt bridges between α1C residues for all three pairwise interactions: $XcpI_p$ D51 to $XcpK_p$ R45, $XcpJ_p$ E58 to $XcpK_p$ R45, and $XcpI_p$ D51 to $XcpJ_p$ E58. (Note that periplasmic domains are designated here with a subscript "p", numbering begins with the first residue of the mature subunit; see Table S1 for amino acid ranges of each construct.) The interaction is also stabilized by salt bridges involving amino acids of $XcpI_p$ α1 and $XcpJ_p$ β11, including $XcpI_p$ D51 and $XcpK_p$ R195. Contacts at the bottom of the bundle of helices lock the ternary complex in place. Double involvement of $XcpI_p$ D51 in $XcpI_p$:J_p and $XcpI_p$:$XcpK_p$ interfaces is evidence to bolster the original

Please cite this article in press as: Escobar et al., Structural interactions define assembly adapter function of a type II secretion system pseudopilin, Structure (2021), https://doi.org/10.1016/j.str.2021.05.015

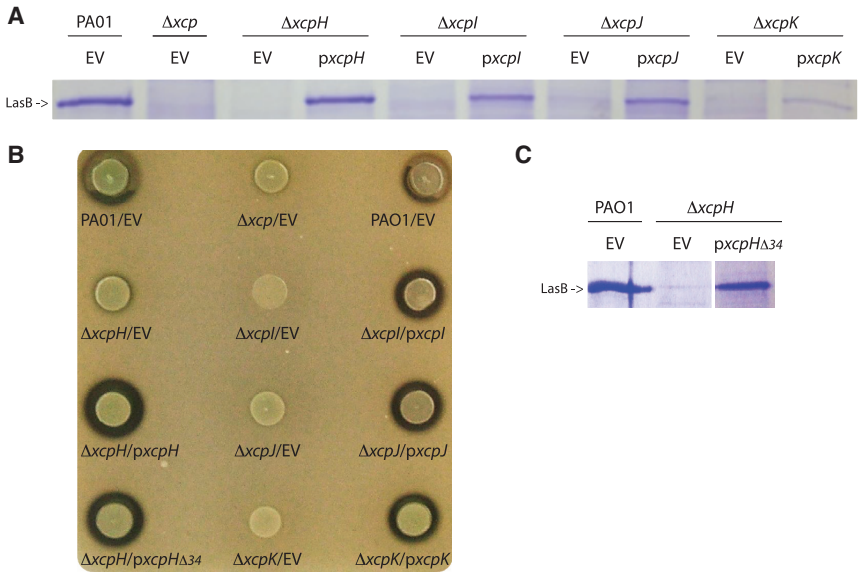

Figure 1. Minor pseudopilins are required for T2S

(A) Secretion of LasB assayed by Coomassie-stained SDS-PAGE of supernatants of PAO1, Δ*xcp* (DZQ40), *ΔxcpH*, *ΔxcpI*, *ΔxcpJ*, and *ΔxcpK* strains harboring empty vector (EV), or complementing plasmid encoding XcpH (p*xcpH*), XcpI (p*xcpI*), XcpJ (p*xcpJ*), or XcpK (p*xcpK*).

(B) LasB protease activity on a skim milk plate is indicated by a casein degradation halo. Colonies representing wild type (PAO1), Δ*xcp*, or complemented Δ*xcp* strains are labeled accordingly. Note that *ΔxcpH* is complemented by p*xcpH* or by pJN105 expressing the XcpH deletion of the β3-β4 loop, p$xcpH_{\Delta 34}$.

(C) Secretion of LasB by *ΔxcpH*/p$xcpH_{\Delta 34}$.

finding that $XcpI_p$ supports the linear organization of $XcpJ_p$:I_p:K_p interactions in the complex (Douzi et al., 2009). Somewhat perplexingly, the largest buried surface area between any two of the soluble proteins in both ternary complexes is between $XcpJ_p$ ($GspJ_p$) and $XcpK_p$ ($GspK_p$), with a total buried surface area of ~3,600 Å^2 in 5VTM. And yet, these two subunits do not interact with each other in solution in the absence of $XcpI_p$ (Douzi et al., 2009).

Several lines of evidence support downward addition of XcpH to the base of the XcpJ:I:K complex through an interaction between globular domains of XcpH and XcpJ. $XcpH_p$ completes the quaternary complex by interacting with $XcpJ_p$ (Douzi et al., 2009). In addition, α1 of XcpH is essential in this interaction and $XcpH_p$ can be positioned most convincingly in a small-angle X-ray scattering envelope of the quaternary complex below $XcpJ_p$ (Zhang et al., 2018). The structural compatibility of the ternary tip complex $GspI_pJ_pK_p$ with downward addition of GspH below GspJ mirrors the suggestion that GspH can be positioned at the top of a GspG fiber but not at the bottom (Korotkov and Hol, 2008; Yanez et al., 2008a). The lack of Glu5 in GspK can also be taken as evidence that GspK does not require helix:helix packing stabilization via a salt bridge with a higher subunit in the filament and thus is located at the top of the pseudopilus (Ng et al., 2016).

In this study we set out to validate the biological importance of XcpH and to decipher the molecular details of the XcpH:I:J:K interaction. Because all data suggest a dynamic and/or small interaction interface, we turned to a collection of compatible techniques suited to interrogation of such interactions. We show that XcpH is indeed critical for efficient T2S in *P. aeruginosa*. We demonstrate that it interacts specifically with the α1 helix of XcpJ, and we narrow the interaction residues to a well-defined interface comprising evolutionarily coupled amino acids in XcpH and XcpJ. Our experimentally determined constraints allow us to synthesize a molecular model of the XcpHIJK quaternary structure, and to place this model in the context of the complete pseudopilus filament, with biological implications for the role of the GspH/XcpH low-abundance pseudopilin. Moreover, the molecular organization involving an inner membrane platform, priming by minor pilins, and a helical subunit assembly is conserved both evolutionarily and structurally in other type IV filamentous nanomachines (Berry and Pelicic, 2015; Denise et al., 2020), including the canonical T4P (Craig et al., 2019; Ng et al., 2016; Nguyen et al., 2015), competence pilus (Dubnau and Blokesch, 2019; Sheppard et al., 2020), and, to some extent the archaellum (Albers and Jarrell, 2018; Braun et al., 2016; Poweleit et al., 2016). Thus our work has wide-ranging implications for understanding the assembly of several fundamental microbial organelles.

RESULTS

The four minor pilins are essential for secretion

In our quest to understand the structure-function relationship of the minor pseudopilin complex, we assessed the independent requirement of each of the four minor pseudopilins of the *P. aeruginosa* Xcp T2SS during the secretion process. In-frame deletion mutants were constructed in the PA01 reference strain for *xcpH*, *xcpI*, *xcpJ*, and *xcpK* (see STAR Methods for nomenclature). Each mutant was assessed for its ability to secrete the major Xcp T2SS effector LasB (Figure 1A) and for the ability of secreted LasB to degrade casein on milk plates (Figure 1B). All four deletion strains were similar in their inability to secrete LasB and lacked protease activity, like the negative control strain missing the entire T2SS operon, thus demonstrating the absolute requirement of each minor pseudopilin in the Xcp T2SS secretion process. This finding is supported by complementation of each secretion-deficient phenotype by introduction of the corresponding wild-type gene on a plasmid. Our data are apparently in conflict with a 2018 publication suggesting that XcpH and XcpK are not required for T2S in *P. aeruginosa* (Zhang et al., 2018). This discrepancy could be due to different experimental procedures or to the use by Zhang et al. of transposon-insertion mutants from an unverified library. Our finding that XcpH is indispensable for secretion prompted us to further explore the 3D integration of XcpH into the XcpHIJK quaternary complex.

Please cite this article in press as: Escobar et al., Structural interactions define assembly adapter function of a type II secretion system pseudopilin, Structure (2021), https://doi.org/10.1016/j.str.2021.05.015

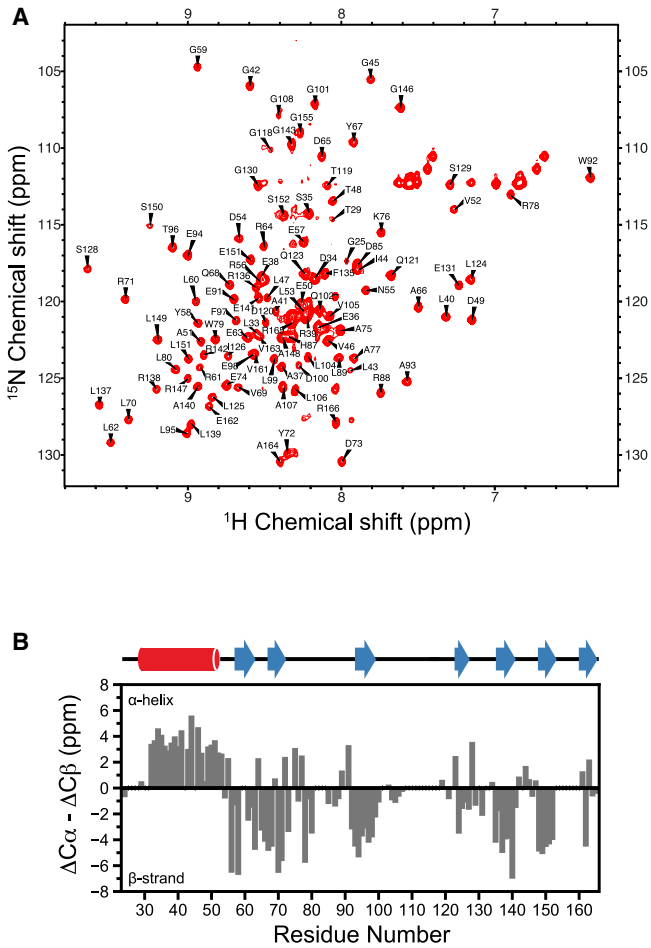

Figure 2. $XcpH_p$ NMR assignments and secondary structure determination

(A) 2D ^{1}H-^{15}N HSQC spectrum showing amino acid assignments.

(B) Secondary chemical shifts were calculated for $XcpH_p$ using α- and β-carbon chemical shifts obtained after backbone sequential assignments. Positive values indicate α helix, while negative values correspond to β strands. Amino acids not assigned or overlapped are represented by a value of zero. Secondary structure elements in the $XcpH_p$ models are shown above.

Chemical-shift perturbation studies of labeled $XcpH_p$ in the presence of $XcpJ_p$

$XcpH_p$ solution NMR assignments

To discover sites of interaction between XcpH and XcpJ, we performed solution NMR experiments. We isotopically labeled the ~16 kDa $XcpH_p$, a feasible NMR target, with ^{15}N and ^{13}C, and carried out amino acid assignments. Regions heavily crowded in the heteronuclear single quantum coherence (HSQC) spectrum were excluded, leading to 85% coverage of the $XcpH_p$ amino acid sequence (Figure 2A). The high signal dispersion of the HSQC spectrum indicates an overall well-folded protein, while the area in the spectrum with high resonance overlap and strong signal (around 8.2 ppm in the ^{1}H dimension and 121 ppm in the ^{15}N dimension) implies a highly dynamic region of the protein.

We employed these assignments to experimentally determine the secondary structure elements within $XcpH_p$ (Figure 2B). Furthermore, we generated two 3D homology models of $XcpH_p$ using PDB: 2KNQ (Zhang and Jin, 2009) and PDB: 2QV8 (Yanez et al., 2008a), which have 38.6% and 36.1% similarity, over 153 or 166 amino acids, to XcpH, respectively. Each 3D model matched our experimental secondary structure assignments well (not shown).

A subset of $XcpH_p$ amino acids, in particular lysines, could not be assigned in our NMR spectra, implying a flexible region of the backbone. We tested the role of these residues in secretion by creating an in-frame deletion of amino acids 108–117, which form a long excursion between β3 and β4, resembling an old-fashioned mouse trap spring in one homology model (Figure S1). We found that *trans*-complementation with the *xcpH*$_{\Delta 34}$ deletion restores LasB secretion and activity to the *ΔxcpH* strain (Figures 1B and 1C). Thus residues 108–117 are not required for LasB secretion, and therefore a disorder-to-order transition of this region cannot be required for secretion of LasB either.

Specific sites of spectral changes along the $XcpH_p$ helix suggest binding interface: chemical-shift perturbation

With $XcpH_p$ chemical shifts in hand, we performed chemical-shift perturbation (CSP) analysis to identify affected structural regions in $XcpH_p$ upon binding of its partner $XcpJ_p$. Resonances from residues close to the protein-protein interface are shifted by the presence of the binding partner. Thus, a sample of 100 μM uniformly ^{15}N-labeled $XcpH_p$ was titrated with increasing amounts of $XcpJ_p$, and the 2D ^{1}H-^{15}N HSQC spectrum was collected. $XcpJ_p$ concentrations above 80 μM displayed significant signal intensity loss due to the large size of the complex. Significant CSPs were observed in multiple places in the amino acid sequence (Figure 3A). By mapping these CSPs on a structural model of $XcpH_p$, we observed one subset of amino acid residues close to the tip of the helical spine of $XcpH_p$ (residues G42 to G59 in α1C, and G130 and G131 on the nearby β4-β5 loop) that are perturbed by the presence of $XcpJ_p$ (Figure 3B). In addition, there is a second set of residues with significant CSP located on the C-terminal β sheet of $XcpH_p$ (residues F135 to R138 in β5, L149 and S153 in β6, and E162 and A164 in β7). These additional perturbed sites may indicate a secondary point of interaction with $XcpJ_p$, or changes in $XcpH_p$ propagated through its structure after binding to $XcpJ_p$. Global smaller amplitude changes across much of $XcpH_p$ suggest that the $XcpH_p$:J_p interaction subtly affects the dynamics or the structure of the entire $XcpH_p$ molecule.

Site-specific cysteine incorporation in $XcpJ_p$ provides $XcpH_p$:J_p interaction sites

Cysteine cross-linking

The knowledge that a significant structural interaction interface for the major pseudopilins is the packing of their α1 helices (Lopez-Castilla et al., 2017), combined with our CSP results implicating the XcpH α1C in the $XcpH_p$:J_p interaction, led us to hypothesize that α1C:α1C packing forms a major interaction between these two minor pseudopilins. We introduced cysteines at surface-exposed α1C positions in $XcpH_p$ (V46, D49, L53) and $XcpJ_p$ (R46, R53) and mixed purified proteins under oxidizing conditions. In every instance, homodimers were formed (Figure 4). Heterodimers between $XcpH_p$ and $XcpJ_p$ were also observed in some prominent cases, most notably for $XcpJ_{R46C}$:H_{L53C} (Figure 4). Heterodimers were weak or absent

Please cite this article in press as: Escobar et al., Structural interactions define assembly adapter function of a type II secretion system pseudopilin, Structure (2021), https://doi.org/10.1016/j.str.2021.05.015

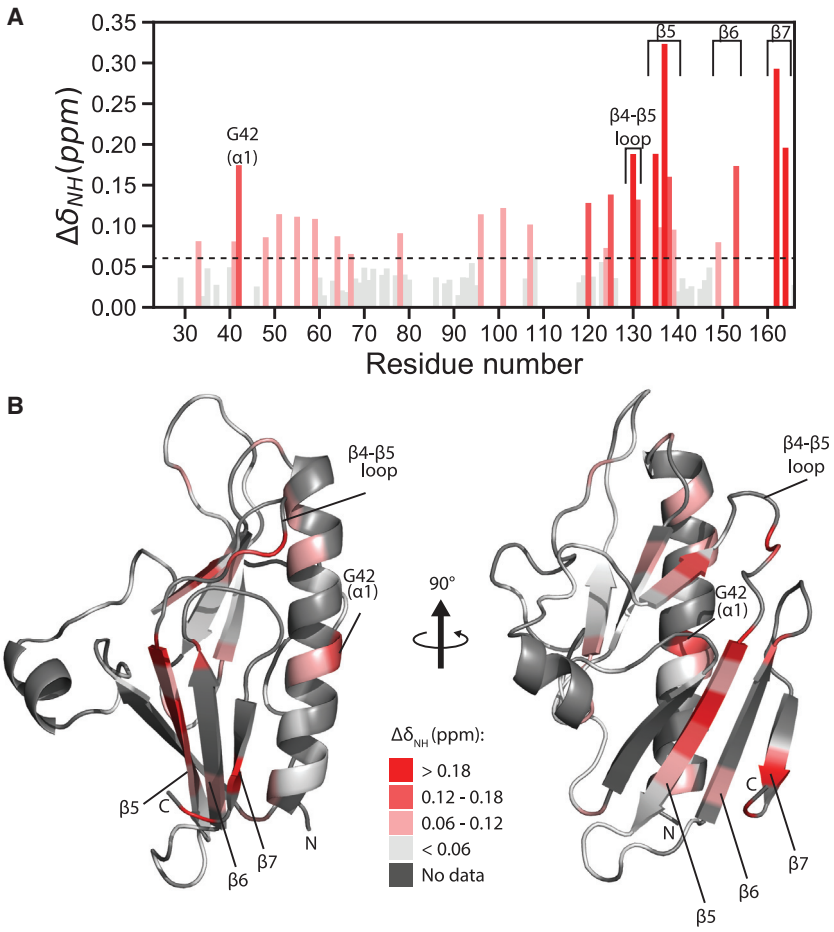

Figure 3. $XcpH_p$ chemical-shift perturbations due to interaction with $XcpJ_p$

(A) CSP values for $XcpH_p$ were calculated using NH chemical-shift differences obtained from the $XcpH_p$ spectrum collected with 0 or 80 μM $XcpJ_p$. CSP values above 0.06 are significant. Value zero corresponds to residues unassigned or overlapped.

(B) CSP values mapped onto an $XcpH_p$ model based on *E. coli* GspH (PDB: 2KNQ). Non-significant changes are white, significant values are depicted in a gradient of red. Amino acids with no data are in gray.

when $XcpH_{pV46C}$ was one of the partners. Although these results provided no quantitative measure of affinity or specificity, they served as motivation to use $XcpJ_p$ α1C cysteine variants as probes of specific sites of interaction in our NMR platform.

Paramagnetic relaxation enhancement

To identify local interactions and specific amino acid involvements in the XcpH:XcpJ interface, we performed paramagnetic relaxation enhancement (PRE) experiments guided by cysteine cross-linking results. In this approach, the effect of a specifically incorporated spin label (1-oxyl-2,2,5,5-tetramethylpyrroline-3-methyl) methanethiosulfonate (MTSL) within $XcpJ_p$ on the ^{15}N $XcpH_p$ spectrum is observed; in particular, $XcpH_p$ residues in proximity to the label on $XcpJ_p$ will experience a decrease in signal intensity. $XcpJ_p$ cysteine variants R46C and R53C were spin labeled, as these positions in $XcpJ_p$ were implicated, in cysteine cross-linking experiments described above, as participating in an XcpH α1C-XcpJ α1C packing interaction. In addition, $XcpH_{pT178C}$ and $XcpH_{pE180C}$ were created and used for spin labeling; these amino acids are on the face of XcpJ opposite α1C, where we did not expect any change in signal from spin-label incorporation. We chose to perform PRE experiments using a 10:3 molar ratio of ^{15}N $XcpH_p$ to spin-labeled $XcpJ_p$ variants. Although a 1:1 ratio would in theory have provided more quantitative results, for this protein pair, it would have led to signal loss as seen in the previously described titration.

MTSL at position 46 or 53 within $XcpJ_p$ has a marked effect on $XcpH_p$ signal intensities (Figure 5A). $XcpJ_{pR46C}$-MTSL induced a signal reduction on $XcpH_p$ α1C (residues 42 to 54), with a maximum effect on D49. Residues located in the loop between $XcpH_p$ β4 and β5 were also affected (G130 and E131) (Figure 5), in agreement with CSP results. $XcpJ_{pR53C}$-MTSL had an effect on similar amino acid residues. Within $XcpH_p$ α1C the overall signal intensity decrease was slightly less compared with the C46 label, but, interestingly, the effect was shifted up the helix, with the residue most greatly affected by the paramagnetic label, $XcpH_p$-N55, located at the tip of $XcpH_p$ (Figure 5). No significant effect was observed on $XcpH_p$ when $XcpJ_p$ was labeled at position T178C or E180C (Figure S2). Thus, the PRE experiment clearly supports that the interface between $XcpH_p$ and $XcpJ_p$ is mediated by α1C interactions with involvement of residues in the β4-β5 loop of XcpH. In addition, the difference in signal intensity decrease and the shift on the most affected residue toward the tip of $XcpH_p$ when the MTSL label is at XcpJ position 53 as opposed to 46 suggest that the helical register is organized with $XcpJ_p$ above $XcpH_p$ in the heterodimer.

Cross-linking mass spectrometry using acidic cross-links via the DMTMM activating reagent

To extend our site-specific information from engineered disulfide bonds and PRE measurements, we applied a recently developed methodology for cross-linking of acidic side chains within a defined distance, followed by mass spectrometry identification of cross-linked peptides (Leitner et al., 2014). We established our pipeline using a 1:1 molar ratio of $XcpH_p$ and $XcpJ_p$ (STAR Methods and Figure S3). Previous work has established that $XcpJ_p$ is indispensable for $XcpH_p$ involvement in the quaternary complex, which was the motivation for using this pair in our NMR experiments, also (Douzi et al., 2009; Zhang et al., 2018). Subsequently, we interrogated the complete quaternary complex of $XcpH_pI_pJ_pK_p$, known already to form *in vitro* a quaternary complex with a molar ratio of 1:1:1:1 (Zhang et al., 2018). These experiments confirmed that the set of acidic cross-links between

Please cite this article in press as: Escobar et al., Structural interactions define assembly adapter function of a type II secretion system pseudopilin, Structure (2021), https://doi.org/10.1016/j.str.2021.05.015

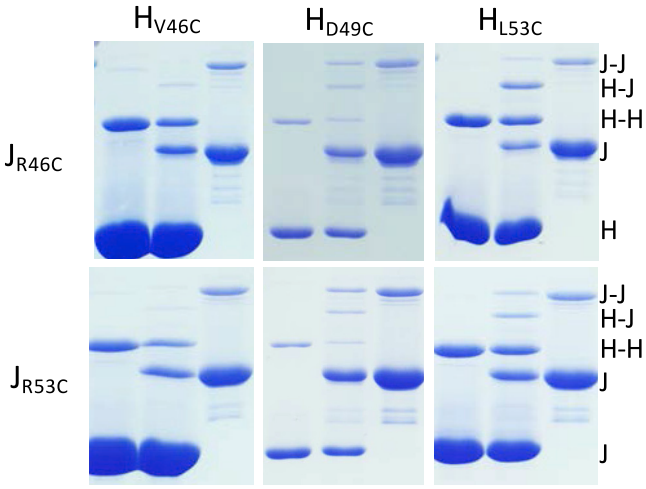

Figure 4. Cysteine cross-linking suggests $XcpH_p$:$XcpJ_p$ α1C packing

Cysteine substitutions were made in the indicated positions within $XcpH_p$ (by column) and in $XcpJ_p$ (by row). Purified proteins were incubated under oxidizing conditions and visualized by Coomassie blue staining of non-reducing SDS-PAGE. In each of the six pairwise combinations, lane 1 is $XcpH_p$ alone, lane 2 is $XcpH_p$ + $XcpJ_p$, and lane 3 is $XcpJ_p$ alone. Monomer, dimer, and heterodimer sizes are indicated along the right-hand side for all three gels in each row.

$XcpH_p$ and $XcpJ_p$ is the same in the heterodimer as in the heterotetramer, and thus we focus on quaternary complex results.

The four minor pseudopilin soluble constructs $XcpH_p$, $XcpI_p$, $XcpJ_p$, and $XcpK_p$ contain 25, 14, 36, and 42 acidic residues, respectively, distributed along their primary sequences. Thus the use of adipic acid dihydrazide (ADH) coupled to 4-(4,6-dimethoxy-1,3,5-triazin-2-yl)-4-methyl-morpholinium chloride (DMTMM) as a coupling reagent appeared promising. DMTMM activates carboxylic acid functionalities, usually poorly reactive, allowing coupling of the cross-linking reagent ADH to the extended amino acid side chains with high efficiency (Leitner et al., 2014). When added in large excess to a freshly prepared aqueous solution containing a 1:1:1:1 molar ratio of $XcpH_p$, $XcpI_p$, $XcpJ_p$, and $XcpK_p$, DMTMM/ADH reagents formed covalent bonds (Figure 6A), which connected proximal acidic functionalities with a maximum linking distance of 20–25 Å (Fajardo et al., 2019). The most likely tetramer band observed on SDS-PAGE of this mixture was excised and analyzed by a classical proteomic bottom-up approach to validate the presence of all four proteins. Each protein was identified unambiguously, with a sequence coverage of 92% for $XcpH_p$ (61 peptides), 78% for $XcpI_p$ (31 peptides), 86% for $XcpJ_p$ (71 peptides), and 91% for $XcpK_p$ (146 peptides).

Due to the long length of the linkers, these cross-links provide complex and valuable information to constrain a model of the quaternary structure of the assembled $XcpH_pI_pJ_pK_p$ complex. Most revealing for our goals of understanding the placement of XcpH within the pseudopilus complex were cross-links between glutamate or aspartate side chains of $XcpH_p$ with any of the other three soluble pseudopilin subunits. Many inter-subunit cross-links between $XcpH_p$ and $XcpJ_p$ were identified between α1C of $XcpH_p$, in particular within the peptide LAGLIGVLTDEAVLDNR, and the several peptides that together span the analogous α1C of $XcpJ_p$ and the β hairpin that follows it (Figures 6B and 6C). An example tandem mass spectrometry spectrum reveals intense peaks defining the connection between the two peptides (Figure 6B), with both chains unambiguously characterized by many fragment ions distributed along the sequences. Moreover, the large mass difference between $y_6\alpha^+$ and $y_7\alpha^+$ characterizes precisely the position of cross-linking. The same α1C region of $XcpH_p$ also cross-links with two regions of $XcpK_p$ and one region of $XcpI_p$, therefore suggesting they are in physical proximity (Figure 6C, Table S3). Interestingly, an acidic residue located in the $XcpH_p$ β4-β5 loop shown by PRE analysis to be in close proximity to the α1C region of $XcpJ_p$ (Figure 5B) is also involved in cross-links with $XcpJ_p$, $XcpI_p$, and $XcpK_p$ (Figure 6C, Table S3).

Cross-links between $XcpI_p$ and $XcpJ_p$ as well as a single cross-link identified between $XcpI_p$ and $XcpK_p$ were all in agreement with the crystallographically determined structures of $GspI_pJ_pK_p$ and $XcpI_pJ_pK_p$. Moreover, intra-subunit cross-links agreed with known protein 3D structures (data not shown). This rich library of cross-links between amino acid side chains within the quaternary complex provides strong constraints for modeling a 3D structure of the $XcpH_pI_pJ_pK_p$ complex.

Integrating experimental data to build quaternary complex model

$XcpH_pI_pJ_pK_p$ complex

Data from spin-labeling studies and acidic cross-linking mass spectrometry were used as restraints on the interaction of $XcpH_p$ with $XcpI_pJ_pK_p$ to model the quaternary complex using HADDOCK software for protein-protein docking. Docking used the structure of the $XcpI_pJ_pK_p$ ternary complex (PDB: 5VTM), the $XcpH_p$ homology model, PRE experimental results, and acidic cross-linking interactions as input (Tables S3 and S4). The best model obtained is in good agreement with these experimental restraints (Figure 7). In this model, the α1C of $XcpH_p$ is in direct contact with that of $XcpJ_p$, and runs approximately parallel to the helical bundle in the $XcpI_pJ_pK_p$ complex. $XcpH_p$ interaction with the ternary complex is maintained by a large network of electrostatic interactions and hydrogen bonds. One group of contacts corresponds to an electrostatic interaction between helices, in particular including a salt bridge between side chains $XcpH_p$ D49 and $XcpJ_p$ R42 (possibly also to $XcpJ_p$ R46, given rotamers available to Arg and resolution of this model) as well as numerous main-chain and side-chain H bonds. A second group comprises β-strand to β-strand contacts. In this interaction, $XcpH_p$ loop β6-β7 G155 and F156 backbone carboxyl groups form hydrogen bonds with $XcpJ_p$ β7 R131 side chain and Q133 main chain, respectively. Other contacts observed between $XcpH_p$ and $XcpJ_p$ correspond to: (1) $XcpH_p$ loop α1-β1 and $XcpJ_p$ loop β4-β5 (N55-R92) and (2) $XcpH_p$ loop β4-β5 and $XcpJ_p$ loop β4-β5 (S129-R92). Remarkably, although no data from the CSP experiments were explicitly included in the HADDOCK restraints, many of the interactions in the model are recapitulated as CSPs; for example, the very high signal interaction within $XcpH_p$ β7 is explained by its close approach to $XcpJ_p$.

The use of acidic cross-linking restraints for $XcpH_p$ with the two other subunits from the quaternary complex disambiguates the $XcpH_p$ position *vis-à-vis* these proteins; for example, the

Please cite this article in press as: Escobar et al., Structural interactions define assembly adapter function of a type II secretion system pseudopilin, Structure (2021), https://doi.org/10.1016/j.str.2021.05.015

CellPress

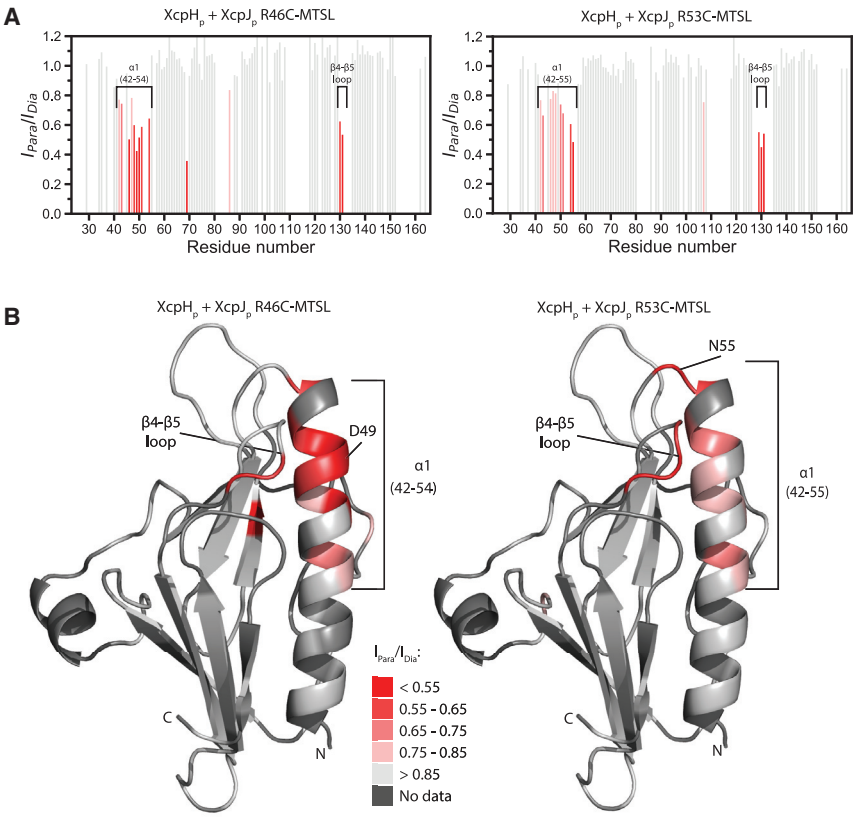

Figure 5. PRE experiments on XcpH$_p$ in the presence of MTSL-labeled XcpJ$_p$

(A) PRE effect of α1C MTSL-labeled XcpJ$_p$ variants on XcpH$_p$ spectra. Significant signal intensity changes are designated with a gradient of red. Residues with no assignments or overlapped have values of zero.

(B) PRE effects of XcpJ$_{pR46C}$-MTSL or XcpJ$_{pR53C}$-MTSL are mapped onto the XcpH$_p$ 3D model.

cross-links to XcpK$_p$ help to position the tip of XcpH$_p$ α1C close to the XcpK$_p$ β sheet, allowing additional contacts that stabilize the complex. These include XcpH$_p$-XcpK$_p$ residues E50-R283, D54-R283, R56-D282, R56-R284, and N55-G309 (Figure 7). We were able to further support this quaternary structure by analyzing the co-evolution of residues in XcpH$_p$ and XcpJ$_p$ (Figure S4). The analysis similarly points to XcpH polar amino acids at the tip of α1C (D49, E57) and in the β4-β5 loop (S128, S129, E131) and pairs them with two sets of XcpJ co-evolved amino acids located within a large flap at the tip of XcpJ (R92 and R99, forming electrostatic interactions) or in the vicinity of α1C (V45, R189, and W107, potentially contributing to packing geometry). This co-evolution result adds credence to the robustness and physiological relevance of our XcpH:XcpJ interaction model. Altogether, we present a model of the XcpH$_p$I$_p$J$_p$K$_p$ quaternary complex supported by experimental evidence, which shows that the interaction of XcpH with XcpJ and XcpK is maintained by several electrostatic interactions.

Filament model

The quaternary complex presented here reveals the interaction of the minor pseudopilin soluble domains and, in particular, places XcpH$_p$ in this ensemble. However, these proteins also interact via their missing hydrophobic α helices (α1N) in the biological context of the pseudopilus. Thus, we used available experimental data and chemically reasonable restraints to model the complete T2SS pseudopilus. For that purpose, hydrophobic α1N was added to the XcpH$_p$I$_p$J$_p$K$_p$ proteins in the soluble quaternary complex model. In addition, the major pseudopilin XcpG filament was modeled using as template the structure of the PulG filament (PDB: 5WDA) (Lopez-Castilla et al., 2017). Then, the quaternary complex was added to the tip of the XcpG filament by aligning XcpH to the first XcpG unit. Finally, the whole model was minimized using PyRosetta (Chaudhury et al., 2010). The best model was selected based on the lowest root-mean-square deviation with respect to the HADDOCK model (Figure 8). An important feature included as a restraint in calculating this model was the salt bridge between N-terminal amino groups and the carboxylic acid of E5 of each preceding unit in the filament, including XcpHIJK at the tip of the pseudopilus. This contact neutralizes these charges in the transmembrane helices as seen in other filament structures such as *P. aeruginosa* PAK pilus (PDB: 5VXY) (Wang et al., 2017). As expected, E5-F1 contacts continue into the minor pseudopilin complex in the following sequence: XcpG-XcpH-XcpJ-XcpI-XcpK. This arrangement maintains the right-handed nature of the major pseudopilin filament structure. In the filament model, the average distance between the E5 carboxyl group and the F1 amino group is 3.58 ± 0.34 Å between adjacent subunits. In addition, Cisneros et al. (Cisneros et al., 2012) showed the close contact between residues 16 and 10 of neighboring subunits (PulJ-PulI and PulI-PulK). Even though these contacts were not used as restraints during modeling, the current model reproduces them between the minor and the major pseudopilins throughout the filament (Figure 8 and not shown). Thus, the Cα-Cα distance from residue 10 to residue 16 of the neighboring subunits in the PulG filament is 8.5 Å; in the model, that distance is on average 8.9 ± 1.4 Å. Strikingly, to maintain the restraint contacts, in particular the E5 to F1 salt bridge between XcpH and XcpJ, it was necessary to allow XcpH α1N between residues 20 and 26 to unravel. Although there is no other experimental evidence that the XcpH helix adopts this melted secondary structure, the equivalent amino acids in the major T2SS pseudopilin and the major T4P pilin are strikingly extended in high-resolution filament models (Kolappan et al., 2016; Lopez-Castilla et al., 2017). In addition, the presence of a glycine at XcpH position 25 supports this conclusion, since glycine and proline residues destabilize α helices.

Another feature observed in the filament model, specifically related to the minor pseudopilin tip, is the capping of each

Please cite this article in press as: Escobar et al., Structural interactions define assembly adapter function of a type II secretion system pseudopilin, Structure (2021), https://doi.org/10.1016/j.str.2021.05.015

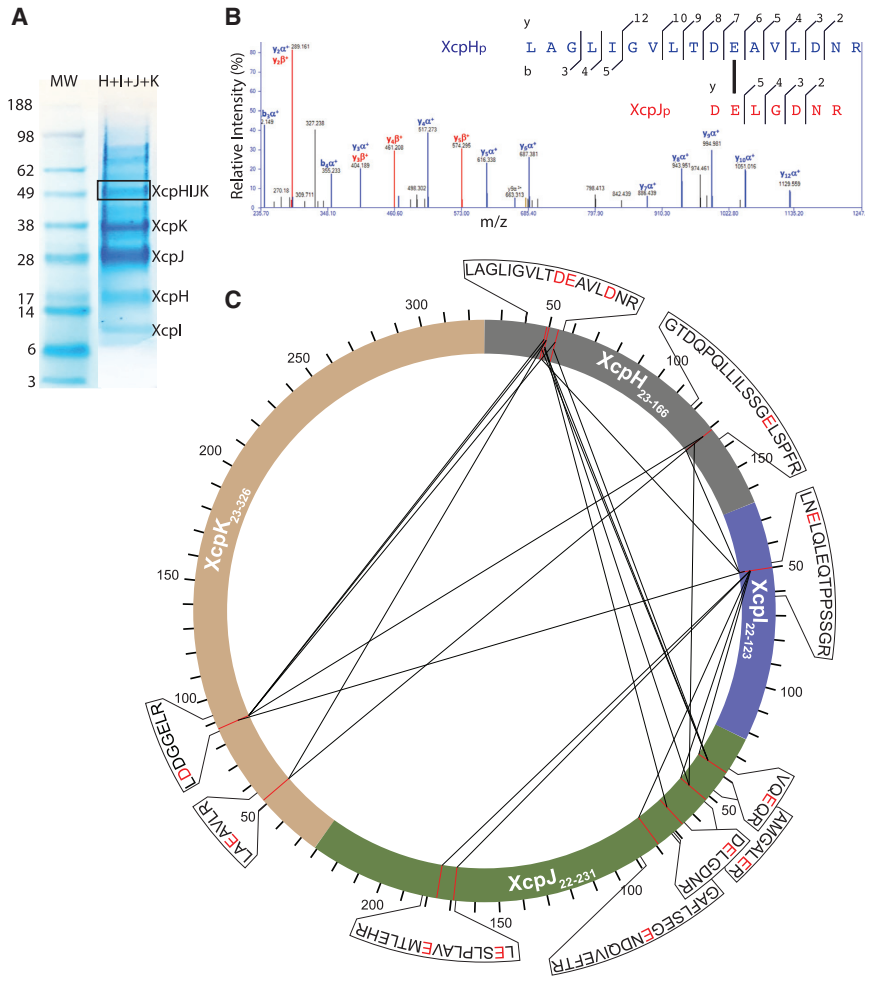

Figure 6. Acidic cross-linking of $XcpH_pI_pJ_pK_p$

(A) SDS-PAGE of cross-linked proteins. Boxed band was identified by proteomics as cross-linked $XcpH_pI_pJ_pK_p$ tetramer.

(B) Tandem mass spectrometry spectrum of a relevant cross-link pair between $XcpH_p$ and $XcpJ_p$. The spectrum shows intense ions identified as y- and b-type ions, allowing unambiguous identification of the two partners (mass accuracy for the parent <2 ppm and for the fragment <10 ppm).

(C) Circular representation of all significant cross-linked pairs detected in the tetramer. (See also Figure S3.)

XcpG protofilament by a minor pseudopilin and the off-center placement of XcpK. If the major pseudopilin filament is separated into four protofilaments, each one is capped by a minor pseudopilin (Figure 8). The exception to this is XcpJ; although the XcpJ globular domain is directly above one protofilament, a small gap exists between XcpJ and the XcpG unit directly below it. An additional consequence of capping one XcpG protofilament with XcpH is that the XcpK globular domain protrudes beyond the major pseudopilin filament diameter, giving the appearance of a hook-like structure to the filament tip (Figure 8).

While our model cannot be considered an atomic structure of the T2SS pseudopilus, it provides a valuable path to testable predictions, such as the importance of XcpH helix unraveling, possible substrate binding sites available on the filament tip, the presence of dynamic contacts between XcpG and minor pseudopilins, and the importance of the XcpK globular domain for secretion.

DISCUSSION

Study of dynamic interactions prioritized by binding affinity is challenging, but we have used chemical, structural, microbiological, and computational approaches to describe the complete ultrastructure of the T2SS pseudopilus and to propose a specific and testable model for the location of the adapter unit XcpH (GspH) between XcpIJK and the filament formed by XcpG. Addition of XcpH would be the next step in a dynamic chronological pathway following XcpIJK association at the periplasmic membrane. Subsequently, XcpG addition absolutely requires the α1N helices, as there is no interaction between the soluble domains of XcpH and XcpG (Figure S5), nor indeed between the soluble domain of XcpG and that of any of the quaternary complex soluble domains individually (Douzi et al., 2009). We have amassed independent and complementary data from several techniques in this integrative study. In particular, the pioneering methodologies in acidic cross-linking represent an important technical breakthrough in the experimental approach to studying protein-protein interactions in multipartner complexes.

This study provides a rationale for the observation that, at least in the *P. aeruginosa* Xcp T2SS, XcpH is required for secretion. It serves as the adapter that connects the regular helical assembly of XcpG subunits to the asymmetric complex that catalyzes initiation of the filament and interacts with substrates and other components of the T2SS. It is possible that XcpH serves other as-yet-unverified roles. For example, given its very strong structural homology to the major XcpG subunit, XcpH might occasionally integrate into the filament and thereby destabilize it, possibly initiating disassembly of the pseudopilus (Ng et al., 2016).

Previous interaction studies using surface plasmon resonance (Douzi et al., 2009) testing pairwise interactions of the soluble domains of XcpG, H, I, J, and K, as well as our current NMR results (Figure S5), reveal that XcpH interacts exclusively with XcpJ. In addition, the binding of XcpH to XcpJ is more efficient when XcpJ is engaged in the XcpIJK ternary complex (Figures 2 and 3 in Douzi et al., 2009). These data suggested that conformational changes in XcpJ upon binding to XcpI and XcpK create a more favorable docking platform for XcpH and/or favor the downward addition of XcpH to the ternary complex over that of XcpG when both are available within the inner membrane. Our

Please cite this article in press as: Escobar et al., Structural interactions define assembly adapter function of a type II secretion system pseudopilin, Structure (2021), https://doi.org/10.1016/j.str.2021.05.015

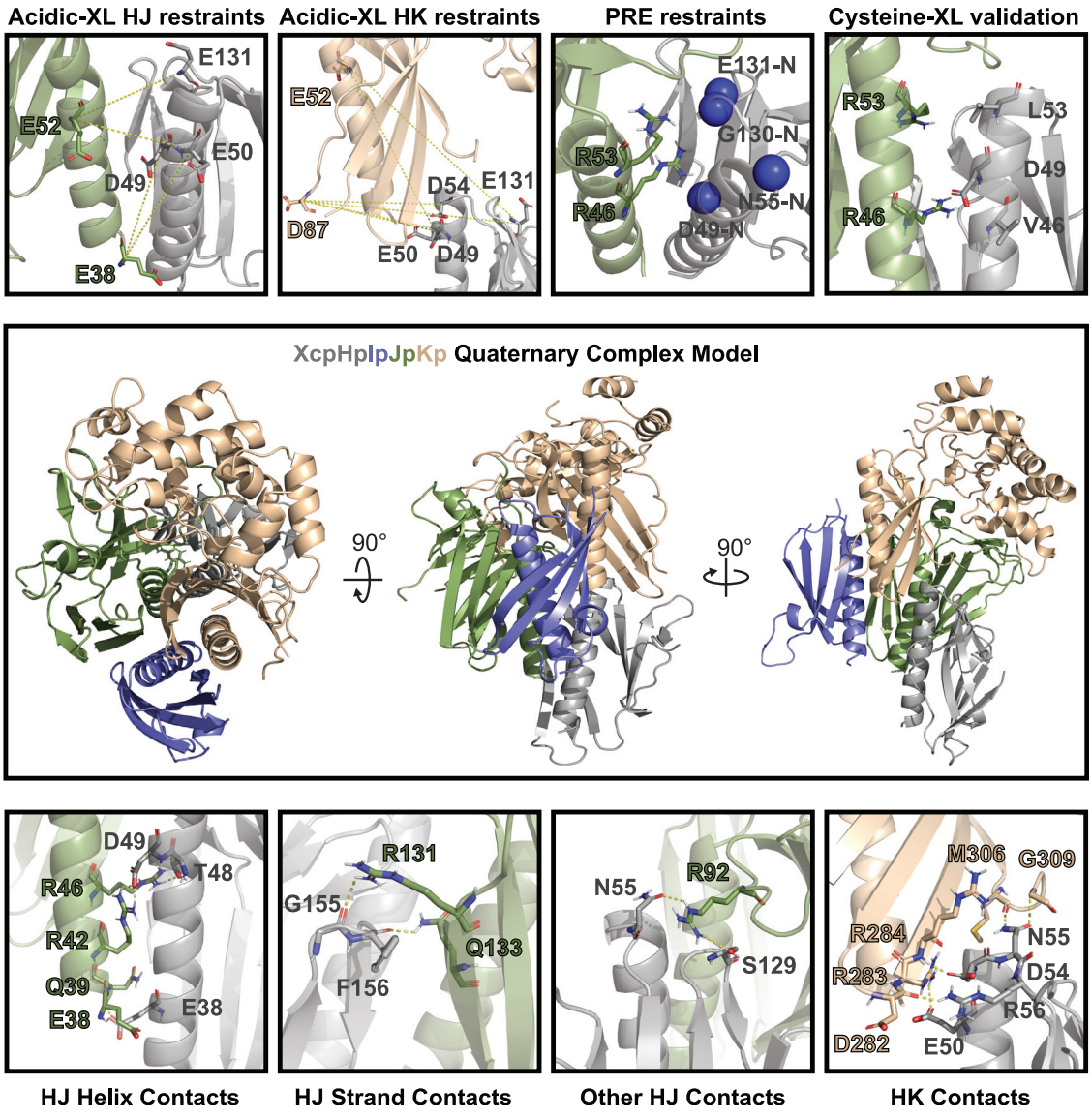

Figure 7. 3D model of $XcpH_pI_pJ_pK_p$

Center: model of the quaternary complex ($XcpH_p$ gray, $XcpI_p$ blue, $XcpJ_p$ green, and $XcpK_p$ wheat) obtained via HADDOCK docking. Top: acidic cross-linking-derived restraints (yellow dotted lines), PRE restraints (spin-labeled residues as sticks and most affected $XcpH_p$ residues as blue spheres at the amide nitrogen), and cysteine proximity validation. Bottom: a subset of predicted side-chain and main-chain interactions from the model, including $XcpH_pJ_p$ salt bridges and hydrogen bonds (yellow dotted lines).

current data supporting many pairwise interactions between minor pseudopilins in the quaternary complex, including between XcpH and each of the other three, fit well with the hypothesis that, alone, the soluble domains have weak and transient interactions, which in some cases are below detection, but that within the full ensemble, these interactions are revealed. Our model furthermore accentuates that the central α helices are, not surprisingly, fundamentally important for more stable interactions. Future experiments will rely on the α1N helical tails being part of the interactions.

Based on the near-atomic resolution of the XcpD secretin (Hay et al., 2017) and taking into account that the pseudopilus tip physically interacts with the secretin (Reichow et al., 2010), a satisfying outcome of our data-driven modeling of the complete pseudopilus is the observation that the filament (~6 nm) docks readily into the periplasm-facing vestibule (~8 nm) (Hay et al., 2017) of the XcpD secretin (Figure S6). Moreover, the positioning of the Xcp pseudopilus plus secretin complex into the cryo-tomographic map of the complete T2SS in its natural context, the bacterial envelope (Ghosal et al., 2019), indicates that 8 to 16 pseudopilin subunits in addition to the tip complex are required to span the periplasm between the inner membrane and the entry into, or the internal periplasmic gate of, the secretin interior, respectively (Figure S6).

Our results provide insights into not only the *P. aeruginosa* T2SS, but indeed into the dozens of T2SS recovered in

Please cite this article in press as: Escobar et al., Structural interactions define assembly adapter function of a type II secretion system pseudopilin, Structure (2021), https://doi.org/10.1016/j.str.2021.05.015

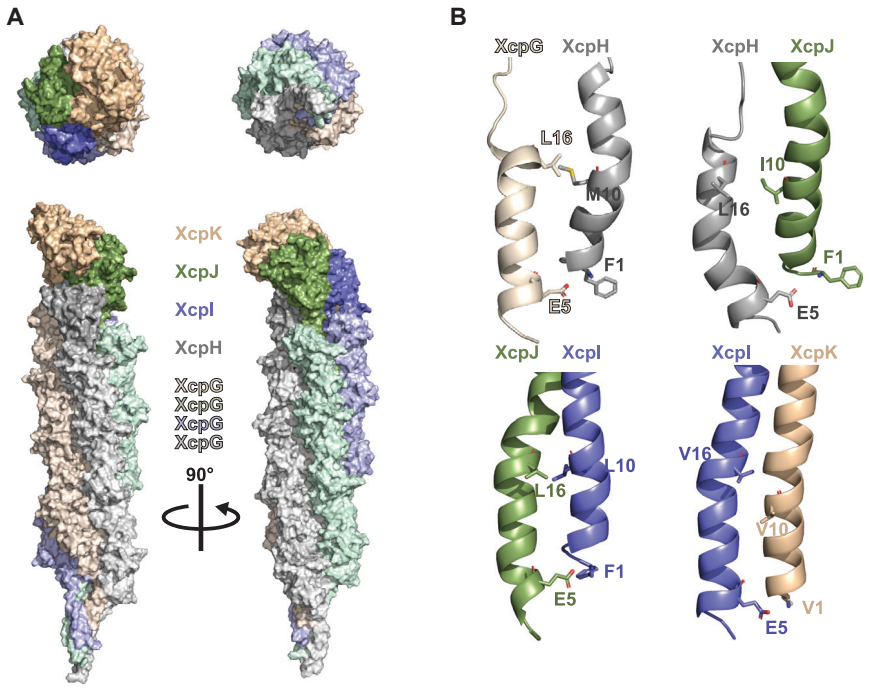

Figure 8. Model of T2SS pseudopilus

(A) XcpHIJK tip complex and XcpG filament shown as a solvent-accessible surface. Top and bottom views (top) and side views (bottom) of the pseudopilus model are shown. Color coding of each XcpG protofilament is a lighter shade of the respective tip subunit color from which it originates.

(B) Transmembrane α1N contacts between neighboring subunits include canonical F1-E5 salt bridge (included as restraint during minimization) and hydrophobic residues at positions 16 and 10 previously described (Cisneros et al., 2012) but *not* used as a modeling restraint. Structure images in Figures 3, 5, 7, and 8 were generated using PyMOL.

proteobacteria with similar genome content of five pre-pseudopilins equivalent to XcpG, H, I, J, and K (Cianciotto and White, 2017). The sequence conservation of these proteins across species implies that their protein-protein interaction interfaces are also conserved, and co-evolved, as shown here for the $XcpH_p$:$XcpJ_p$ interface. By extension, both the minor pseudopilins of the T2SS and the minor pilins of the T4P can be expected to form a similar quaternary complex in which an adapter minor (pseudo)pilin subunit sets the stage for downward addition of the major (pseudo)pilin subunit to form the extended filament by interacting via its periplasmic domain with the three upper minor subunits and via its unraveled α1C with the first major subunit. Correspondingly, the set of *E. coli* T4P minor pilins restores assembly of the major T2SS pseudopilin PulG in the absence of minor pseudopilins PulHJIK (Cisneros et al., 2012). An open question is whether the secretion ATPase motor protein, GspE, is required for insertion and/or α1C unraveling in this adapter minor pilin at the junction between the tip complex and the filament itself.

STAR★METHODS

Detailed methods are provided in the online version of this paper and include the following:

- KEY RESOURCES TABLE
- RESOURCE AVAILABILITY
  - Lead contact
  - Materials availability
  - Data and code availability
- EXPERIMENTAL MODEL AND SUBJECT DETAILS
  - Bacterial strains and plasmids
- METHOD DETAILS
  - Gene and protein nomenclature
  - LasB secretion and protease activity on plates
  - Protein production and purification
  - *In vitro* cysteine cross-linking
  - Acidic cross-linking of $XcpH_p$ + $XcpJ_p$ and $XcpH_p$ + $XcpI_p$ + $XcpJ_p$ + $XcpK_p$
  - NMR experiments
  - Quaternary complex computational modeling
  - Biological filament modeling
  - Positioning of the pseudopilus into secretin and T2SS maps
  - Evolutionarily coupled residues between $XcpH_p$ and $XcpJ_p$
- QUANTIFICATION AND STATISTICAL ANALYSIS
  - Cross-linking data analysis

SUPPLEMENTAL INFORMATION

Supplemental information can be found online at https://doi.org/10.1016/j.str.2021.05.015.

ACKNOWLEDGMENTS

We thank Dr. E. Durand for pET-$XcpG_p$ plasmid construction, Mrs. N. Tanteliarisoa for help in the preparation of acidic cross-linking samples, and Dr. Lisa Craig for valuable comments. We acknowledge funding from the ANR to R.V. (ANR-14-CE09-0027-01 and ANR-19-CE11-0020-01) and from the UW-Madison Center for Interdisciplinary French Studies and the US National Science Foundation to K.T.F. (IOS 1353674). Mass spectrometers used in this work were supported by the Walloon Region (Belgium) and the European Regional Development Fund. This study made use of the National Magnetic Resonance Facility at Madison, which is supported by NIH grant P41GM103399 (NIGMS). Equipment was purchased with funds from UW-Madison, the NIH (P41GM103399, S10RR02781, S10RR08438, S10RR023438, S10RR025062, S10RR029220), the NSF (DMB-8415048, OIA-9977486, BIR-9214394), and the USDA.

AUTHOR CONTRIBUTIONS

R.V., L.Q., and K.T.F. conceived the studies. C.A.E. and B.D. did cloning and purified proteins. C.A.E. carried out CSP and PRE experiments and quaternary structure and filament modeling. B.D. performed cysteine cross-linking experiments. G.B. constructed *P. aeruginosa* strains and did secretion assays. B.B. led co-evolution calculations. S.A. carried out NMR experiments in Figure S5. L.Q. performed acidic cross-linking methods development and experiments. R.V., K.T.F., and C.A.E. drafted the manuscript. All authors edited the manuscript and prepared the figures.

DECLARATION OF INTERESTS

The authors declare no competing interests.

Received: December 23, 2020
Revised: March 15, 2021
Accepted: May 28, 2021
Published: June 16, 2021

REFERENCES

Albers, S.-V., and Jarrell, K.F. (2018). The archaellum: an update on the unique archaeal motility structure. Trends Microbiol. *26*, 351–362.

Alphonse, S., Durand, E., Douzi, B., Waegele, B., Darbon, H., Filloux, A., Voulhoux, R., and Bernard, C. (2010). Structure of the Pseudomonas aeruginosa XcpT pseudopilin, a major component of the type II secretion system. J. Struct. Biol. *169*, 75–80.

Ball, G., Chapon-Hervé, V., Bleves, S., Michel, G., and Bally, M. (1999). Assembly of XcpR in the cytoplasmic membrane is required for extracellular protein secretion in *Pseudomonas aeruginosa*. J. Bacteriol. *181*, 382–388.

Bally, M., Filloux, A., Akrim, M., Ball, G., Lazdunski, A., and Tommassen, J. (1992). Protein secretion in Pseudomonas aeruginosa: characterization of seven xcp genes and processing of secretory apparatus components by prepilin peptidase. Mol. Microbiol. *6*, 1121–1131.

Berry, J.L., and Pelicic, V. (2015). Exceptionally widespread nanomachines composed of type IV pilins: the prokaryotic Swiss Army knives. FEMS Microbiol. Rev. *39*, 134–154.

Berman, H.M., Adams, P.D., Bonvin, A.A., Burley, S.K., Carragher, B., Chiu, W., DiMaio, F., Ferrin, T.E., Gabanyi, M.J., Goddard, T.D., et al. (2019). Federating structural models and data: outcomes from A workshop on archiving integrative structures. Structure *27*, 1745–1759.

Bleves, S., Voulhoux, R., Michel, G., Lazdunski, A., Tommassen, J., and Filloux, A. (1998). The secretion apparatus of Pseudomonas aeruginosa: identification of a fifth pseudopilin, XcpX (GspK family). Mol. Microbiol. *27*, 31–40.

Braun, T., Vos, M.R., Kalisman, N., Sherman, N.E., Rachel, R., Wirth, R., Schröder, G.F., and Egelman, E.H. (2016). Archaeal flagellin combines a bacterial type IV pilin domain with an Ig-like domain. Proc. Natl. Acad. Sci. U S A *113*, 10352–10357.

Chang, Y.-W., Rettberg, L.A., Treuner-Lange, A., Iwasa, J., Søgaard-Andersen, L., and Jensen, G.J. (2016). Architecture of the type IVa pilus machine. Science *351*, aad2001.

Chaudhury, S., Lyskov, S., and Gray, J.J. (2010). PyRosetta: a script-based interface for implementing molecular modeling algorithms using Rosetta. Bioinformatics *26*, 689–691.

Chernyatina, A.A., and Low, H.H. (2019). Core architecture of a bacterial type II secretion system. Nat. Commun. *10*, 5437.

Cianciotto, N.P., and White, R.C. (2017). Expanding role of type II secretion in bacterial pathogenesis and beyond. Infect. Immun. *85*, e00014–17.

Cisneros, D.A., Bond, P.J., Pugsley, A.P., Campos, M., and Francetic, O. (2012). Minor pseudopilin self-assembly primes type II secretion pseudopilus elongation. EMBO J. *31*, 1041–1053.

Craig, L., Forest, K.T., and Maier, B. (2019). Type IV pili: dynamics, biophysics and functional consequences. Nat. Rev. Microbiol. *17*, 429–440.

Delaglio, F., Grzesiek, S., Vuister, G.W., Zhu, G., Pfeifer, J., and Bax, A. (1995). NMRPipe: a multidimensional spectral processing system based on UNIX pipes. J. Biomol. NMR *6*, 277–293.

Denise, R., Abby, S.S., and Rocha, E.P.C. (2020). The evolution of protein secretion systems by Co-option and tinkering of cellular machineries. Trends Microbiol. *28*, 372–386.

Douzi, B., Durand, E., Bernard, C., Alphonse, S., Cambillau, C., Filloux, A., Tegoni, M., and Voulhoux, R. (2009). The XcpV/GspI pseudopilin has a central role in the assembly of a quaternary complex within the T2SS pseudopilus. J. Biol. Chem. *284*, 34580–34589.

Douzi, B., Ball, G., Cambillau, C., Tegoni, M., and Voulhoux, R. (2011). Deciphering the Xcp Pseudomonas aeruginosa type II secretion machinery through multiple interactions with substrates. J. Biol. Chem. *286*, 40792–40801.

Dubnau, D., and Blokesch, M. (2019). Mechanisms of DNA uptake by naturally competent bacteria. Annu. Rev. Genet. *53*, 217–237.

Durand, E., Michel, G., Voulhoux, R., Kurner, J., Bernadac, A., and Filloux, A. (2005). XcpX controls biogenesis of the Pseudomonas aeruginosa XcpT-containing pseudopilus. J. Biol. Chem. *280*, 31378–31389.

Evdokimov, A.G., Phan, J., Tropea, J.E., Routzahn, K.M., Peters, H.K., Pokross, M., and Waugh, D.S. (2003). Similar modes of polypeptide recognition by export chaperones in flagellar biosynthesis and type III secretion. Nat. Struct. Biol. *10*, 789–793.

Fajardo, J.E., Shrestha, R., Gil, N., Belsom, A., Crivelli, S.N., Czaplewski, C., Fidelis, K., Grudinin, S., Karasikov, M., Karczyńska, A.S., et al. (2019). Assessment of chemical-crosslink-assisted protein structure modeling in CASP13. Proteins *87*, 1283–1297.

Franz, L.P., Douzi, B., Durand, E., Dyer, D.H., Voulhoux, R., and Forest, K.T. (2011). Structure of the minor pseudopilin XcpW from the Pseudomonas aeruginosa type II secretion system. Acta Crystallogr. Biol. Crystallogr. *67*, 124–130.

Fürste, J.P., Pansegrau, W., Frank, R., Blöcker, H., Scholz, P., Bagdasarian, M., and Lanka, E. (1986). Molecular cloning of the plasmid RP4 primase region in a multi-host-range tacP expression vector. Gene *48*, 119–131.

Ghosal, D., Kim, K.W., Zheng, H., Kaplan, M., Truchan, H.K., Lopez, A.E., McIntire, I.E., Vogel, J.P., Cianciotto, N.P., and Jensen, G.J. (2019). In vivo structure of the Legionella type II secretion system by electron cryotomography. Nat. Microbiol. *4*, 2101–2108.

Gu, S., Shevchik, V.E., Shaw, R., Pickersgill, R.W., and Garnett, J.A. (2017). The role of intrinsic disorder and dynamics in the assembly and function of the type II secretion system. Biochim. Biophys. Acta Proteins Proteom. *1865*, 1255–1266.

Hay, I.D., Belousoff, M.J., and Lithgow, T. (2017). Structural basis of type 2 secretion system engagement between the inner and outer bacterial membranes. MBio *8*, e01344-17.

Hay, I.D., Belousoff, M.J., Dunstan, R.A., Bamert, R.S., and Lithgow, T. (2018). Structure and membrane topography of the vibrio-type secretin complex from the type 2 secretion system of enteropathogenic Escherichia coli. J. Bacteriol. *200*, e00521–17.

Hopf, T.A., Schärfe, C.P.I., Rodrigues, J.P.G.L.M., Green, A.G., Kohlbacher, O., Sander, C., Bonvin, A.M.J.J., and Marks, D.S. (2014). Sequence co-evolution gives 3D contacts and structures of protein complexes. ELife *3*, e03430.

Hu, N.-T., Leu, W.-M., Lee, M.-S., Chen, A., Chen, S.-C., Song, Y.-L., and Chen, L.-Y. (2002). XpsG, the major pseudopilin in Xanthomonas campestris pv. campestris, forms a pilus-like structure between cytoplasmic and outer membranes. Biochem. J. *365*, 205–211.

Jeong, J.-Y., Yim, H.-S., Ryu, J.-Y., Lee, H.S., Lee, J.-H., Seen, D.-S., and Kang, S.G. (2012). One-step sequence- and ligation-independent cloning as a rapid and versatile cloning method for functional genomics studies. Appl. Environ. Microbiol. *78*, 5440–5443.

Kelley, L.A., Mezulis, S., Yates, C.M., Wass, M.N., and Sternberg, M.J. (2015). The Phyre2 web portal for protein modeling, prediction and analysis. Nat. Protoc. *10*, 845–858.

Kolappan, S., Coureuil, M., Yu, X., Nassif, X., Egelman, E.H., and Craig, L. (2016). Structure of the Neisseria meningitidis Type IV pilus. Nat. Commun. *7*, 13015.

Korotkov, K.V., and Hol, W.G.J. (2008). Structure of the GspK-GspI-GspJ complex from the enterotoxigenic Escherichia coli type 2 secretion system. Nat. Struct. Mol. Biol. *15*, 462–468.

Korotkov, K.V., and Sandkvist, M. (2019). Architecture, function, and substrates of the type II secretion system. EcoSal Plus *8*. https://doi.org/10.1128/ecosalplus.ESP-0034-2018.

Lam, A.Y., Pardon, E., Korotkov, K.V., Hol, W.G.J., and Steyaert, J. (2009). Nanobody-aided structure determination of the EpsI:EpsJ pseudopilin heterodimer from Vibrio vulnificus. J. Struct. Biol. *166*, 8–15.

Lasica, A.M., Ksiazek, M., Madej, M., and Potempa, J. (2017). The type IX secretion system (T9SS): highlights and recent insights into its structure and function. Front. Cell. Infect. Microbiol. *7*, 215.

Lee, W., Tonelli, M., and Markley, J.L. (2015). NMRFAM-SPARKY: enhanced software for biomolecular NMR spectroscopy. Bioinformatics *31*, 1325–1327.

Leitner, A., Joachimiak, L.A., Unverdorben, P., Walzthoeni, T., Frydman, J., Förster, F., and Aebersold, R. (2014). Chemical cross-linking/mass spectrometry targeting acidic residues in proteins and protein complexes. Proc. Natl. Acad. Sci. U S A *111*, 9455–9460.

Lima, D.B., de Lima, T.B., Balbuena, T.S., Neves-Ferreira, A.G.C., Barbosa, V.C., Gozzo, F.C., and Carvalho, P.C. (2015). SIM-XL: a powerful and user-friendly tool for peptide cross-linking analysis. J. Proteomics *129*, 51–55.

Lopez-Castilla, A., Thomassin, J.L., Bardiaux, B., Zheng, W., Nivaskumar, M., Yu, X., Nilges, M., Egelman, E.H., Izadi-Pruneyre, N., and Francetic, O. (2017). Structure of the calcium-dependent type 2 secretion pseudopilus. Nat. Microbiol. *2*, 1686–1695.

McLaughlin, L.S., Haft, R.J.F., and Forest, K.T. (2012). Structural insights into the Type II secretion nanomachine. Curr. Opin. Struct. Biol. *22*, 208–216.

Newman, J.R., and Fuqua, C. (1999). Broad-host-range expression vectors that carry the L-arabinose-inducible Escherichia coli araBAD promoter and the araC regulator. Gene *227*, 197–203.

Ng, D., Harn, T., Altindal, T., Kolappan, S., Marles, J.M., Lala, R., Spielman, I., Gao, Y., Hauke, C.A., Kovacikova, G., et al. (2016). The Vibrio cholerae minor pilin TcpB initiates assembly and retraction of the toxin-coregulated pilus. PLoS Pathog. *12*, e1006109.

Nguyen, Y., Sugiman-Marangos, S., Harvey, H., Bell, S.D., Charlton, C.L., Junop, M.S., and Burrows, L.L. (2015). Pseudomonas aeruginosa minor pilins prime type IVa pilus assembly and promote surface display of the PilY1 adhesin. J. Biol. Chem. *290*, 601–611.

Nivaskumar, M., Santos-Moreno, J., Malosse, C., Nadeau, N., Chamot-Rooke, J., Tran Van Nhieu, G., and Francetic, O. (2016). Pseudopilin residue E5 is essential for recruitment by the type 2 secretion system assembly platform. Mol. Microbiol. *101*, 924–941.

Nunn, D.N., and Lory, S. (1993). Cleavage, methylation, and localization of the Pseudomonas aeruginosa export proteins XcpT, -U, -V, and -W. J. Bacteriol. *175*, 4375–4382.

Parge, H.E., Forest, K.T., Hickey, M.J., Christensen, D.A., Getzoff, E.D., and Tainer, J.A. (1995). Structure of the fibre-forming protein pilin at 2.6 A resolution. Nature *378*, 32–38.

Pasloske, B.L., Scraba, D.G., and Paranchych, W. (1989). Assembly of mutant pilins in Pseudomonas aeruginosa: formation of pili composed of heterologous subunits. J. Bacteriol. *171*, 2142–2147.

Poweleit, N., Ge, P., Nguyen, H.H., Loo, R.R.O., Gunsalus, R.P., and Zhou, Z.H. (2016). CryoEM structure of the Methanospirillum hungatei archaellum reveals structural features distinct from the bacterial flagellum and type IV pilus. Nat. Microbiol. *2*, 16222.

Reichow, S.L., Korotkov, K.V., Hol, W.G.J., and Gonen, T. (2010). Structure of the cholera toxin secretion channel in its closed state. Nat. Struct. Mol. Biol. *17*, 1226–1232.

Schrödinger, L., and DeLano, W. (2020). PyMOL. http://www.pymol.org/pymol.

Sheppard, D., Berry, J.-L., Denise, R., Rocha, E.P.C., Matthews, S., and Pelicic, V. (2020). The major subunit of widespread competence pili exhibits a novel and conserved type IV pilin fold. J. Biol. Chem. *295*, 6594–6604.

Studier, F.W. (2014). Stable expression clones and auto-induction for protein production in E. coli. In Structural Genomics: Methods and Protocols (Springer), pp. 17–22.

Sysoeva, T.A., Zepeda-Rivera, M.A., Huppert, L.A., and Burton, B.M. (2014). Dimer recognition and secretion by the ESX secretion system in Bacillus subtilis. Proc. Natl. Acad. Sci. U S A *111*, 7653–7658.

Tamiola, K., Acar, B., and Mulder, F.A.A. (2010). Sequence-specific random coil chemical shifts of intrinsically disordered proteins. J Am Chem Soc 132, 18000–18003.

Thomassin, J.-L., Santos Moreno, J., Guilvout, I., Tran Van Nhieu, G., and Francetic, O. (2017). The trans-envelope architecture and function of the type 2 secretion system: new insights raising new questions. Mol. Microbiol. *105*, 211–226.

Treuner-Lange, A., Chang, Y.-W., Glatter, T., Herfurth, M., Lindow, S., Chreifi, G., Jensen, G.J., and Søgaard-Andersen, L. (2020). PilY1 and minor pilins form a complex priming the type IVa pilus in Myxococcus xanthus. Nat. Commun. *11*, 5054.

Trokter, M., and Waksman, G. (2018). Translocation through the conjugative type IV secretion system requires unfolding of its protein substrate. J. Bacteriol. *200*, e00615–e00617.

Viarre, V., Cascales, E., Ball, G., Michel, G.P.F., Filloux, A., and Voulhoux, R. (2009). HxcQ liposecretin is self-piloted to the outer membrane by its N-terminal lipid anchor. J. Biol. Chem. *284*, 33815–33823.

Vignon, G., Köhler, R., Larquet, E., Giroux, S., Prévost, M.-C., Roux, P., and Pugsley, A.P. (2003). Type IV-like pili formed by the type II secreton: specificity, composition, bundling, polar localization, and surface presentation of peptides. J. Bacteriol. *185*, 3416–3428.

Wang, F., Coureuil, M., Osinski, T., Orlova, A., Altindal, T., Gesbert, G., Nassif, X., Egelman, E.H., and Craig, L. (2017). Cryoelectron microscopy reconstructions of the *Pseudomonas aeruginosa* and *Neisseria gonorrhoeae type* IV pili at sub-nanometer resolution. Structure *25*, 1423–1435.

Yan, Z., Yin, M., Xu, D., Zhu, Y., and Li, X. (2017). Structural insights into the secretin translocation channel in the type II secretion system. Nat. Struct. Mol. Biol. *24*, 177–183.

Yanez, M.E., Korotkov, K.V., Abendroth, J., and Hol, W.G. (2008a). Structure of the minor pseudopilin EpsH from the Type 2 secretion system of Vibrio cholerae. J. Mol. Biol. *377*, 91–103.

Yanez, M.E., Korotkov, K.V., Abendroth, J., and Hol, W.G. (2008b). The crystal structure of a binary complex of two pseudopilins: EpsI and EpsJ from the type 2 secretion system of Vibrio vulnificus. J. Mol. Biol. *375*, 471–486.

Zhang, Y., and Jin, C. (2009). Solution Structure of E.Coli GspH. Protein Data Bank Unpublished Entry 2KNQ (Protein Data Bank).

Zhang, Y., Faucher, F., Zhang, W., Wang, S., Neville, N., Poole, K., Zheng, J., and Jia, Z. (2018). Structure-guided disruption of the pseudopilus tip complex inhibits the Type II secretion in Pseudomonas aeruginosa. PLoS Pathog. *14*, e1007343.

van Zundert, G.C.P., Rodrigues, J.P.G.L.M., Trellet, M., Schmitz, C., Kastritis, P.L., Karaca, E., Melquiond, A.S.J., van Dijk, M., de Vries, S.J., and Bonvin, A.M.J.J. (2016). The HADDOCK2.2 web server: user-friendly integrative modeling of biomolecular complexes. J. Mol. Biol. *428*, 720–725.

Please cite this article in press as: Escobar et al., Structural interactions define assembly adapter function of a type II secretion system pseudopilin, Structure (2021), https://doi.org/10.1016/j.str.2021.05.015

CellPress

STAR★METHODS

KEY RESOURCES TABLE

REAGENT or RESOURCE	SOURCE	IDENTIFIER
Bacterial and virus strains		
E. coli K-12 DH5α	Laboratory collection	N/A
E. coli BL21(DE3) pLysS	Laboratory collection	N/A
P. aeruginosa PAO1 WT	Laboratory collection	N/A
P. aeruginosa PAO1 *ΔxcpH*	This study	N/A
P. aeruginosa PAO1 *ΔxcpI*	This study	N/A
P. aeruginosa PAO1 *ΔxcpJ*	Franz et al., 2011	N/A
P. aeruginosa PAO1 *ΔxcpK*	Bleves et al., 1998	N/A
P. aeruginosa PAO1 *Δxcp or DZQ40*	Ball et al., 1999	N/A
Chemicals, peptides, and recombinant proteins		
^{15}N-U ammonium chloride	Cambridge Isotope Laboratories	Cat# NLM-467-1
^{13}C-U glucose	Cambridge Isotope Laboratories	Cat# CLM-1396-2
Ni-NTA agarose resin	Qiagen	Cat# 30210
6xHis-TEV protease	Prepared In-Lab	N/A
Adipic acid dihydrazide (ADH)	Sigma Aldrich (Merck)	Cat#A0638
4-(4,6-dimethoxy-1,3,5-triazin-2-yl)-4-methyl-morpholinium chloride (DMTMM)	Sigma Aldrich (Merck)	Cat# 74104
NuPageTM	Invitrogen	Cat# NP0322PK2
Lys-C Protease Pierce, MS grade	ThermoFisher Scientific	Cat# 90307
Trypsin Protease Pierce	ThermoFisher Scientific	Cat# 90058
2,2-dimethyl-2-silapentane-5-sulfonate (DSS)	Sigma	Cat# 178837-1G
1-Oxyl-2,2,5,5-tetramethylpyrroline-3-methyl) methanethiosulfonate (MTSL)	Santa Cruz Biotechnology	Cat# SC-208677
XcpHp, XcpJp, XcpJp, XcpKp	This study	N/A
$XcpH_{pV46C}$, $XcpH_{pD49C}$, $XcpH_{pL53C}$	This study	N/A
$XcpJ_{pR46C}$, $XcpJ_{pR53C,}$ $XcpJ_{pT178C}$, $XcpJ_{pE180C}$	This study	N/A
Deposited data		
E. coli GspH	Zhang and Jin, 2009	https://www.rcsb.org PDB: 2KNQ
V. cholera EpsH	Yanez et al., 2008a	https://www.rcsb.org PDB: 2QV8
P. aeruginosa XcpIJK ternary complex	Zhang et al., 2018	https://www.rcsb.org PDB: 5VTM
PulG filament cryoEM reconstruction	Lopez-Castilla et al., 2017	https://www.rcsb.org PDB: 5WDA
NMR structure of XcpT	Alphonse et al., 2010	https://www.rcsb.org PDB: 2KEP
P. aeruginosa Type IV pilus cryoEM reconstruction	Wang et al., 2017	https://www.rcsb.org PDB: 5VXY
ETEC GspIJK ternary complex	Korotkov and Hol, 2008	https://www.rcsb.org PDB: 3CI0
NMR Data for XcpH, XcpH + XcpJ CSP, XcpH + XcpJ PRE	This study	https://bmrb.io BMRB 50449
Acidic Crosslinking Mass Spectrometry Dataset for XcpH & XcpI	This study	https://massive.ucsd.edu/ #MSV000086916

(*Continued on next page*)

Please cite this article in press as: Escobar et al., Structural interactions define assembly adapter function of a type II secretion system pseudopilin, Structure (2021), https://doi.org/10.1016/j.str.2021.05.015

Continued

REAGENT or RESOURCE	SOURCE	IDENTIFIER
Acidic Crosslinking Mass Spectrometry Dataset for quaternary complex	This study	https://massive.ucsd.edu/ #MSV000086915
$XcpH_pI_pJ_pK_p$ quaternary complex	This study	https://pdb-dev.wwpdb.org PDBDEV_00000086
XcpGHIJK pseudopilus filament structural model	This study	https://pdb-dev.wwpdb.org PDBDEV_00000087
Oligonucleotides		
Twelve mutagenic primers, listed in Table S2	Integrated DNA Technologies	N/A
Recombinant DNA		
pETG-20A	A. Gerloof (EMBL)	N/A
pETG-20A-$XcpH_p$	Douzi et al., 2009	N/A
pETG-20A-$XcpI_p$	Douzi et al., 2009	N/A
pETG-20A-$XcpJ_p$	Douzi et al., 2009	N/A
pETG-20A-$XcpK_p$	Douzi et al., 2009	N/A
pETG-20A-$XcpH_{pV46C}$	This Study	N/A
pETG-20A-$XcpH_{pD49C}$	This Study	N/A
pETG-20A-$XcpH_{pL53C}$	This Study	N/A
pETG-20A-$XcpJ_{pR46C}$	This Study	N/A
pETG-20A-$XcpJ_{pR53C}$	This Study	N/A
pETG-20A-$XcpJ_{pT178C}$	This Study	N/A
pETG-20A-$XcpJ_{pE180C}$	This Study	N/A
pET-XcpGp	Durand et al., 2005	N/A
pET-XcpHp	This Study	N/A
pJN105	Newman and Fuqua, 1999	N/A
p*xcpH*	This Study	N/A
p$xcpH_{\Delta 34}$	This Study	N/A
pMMB	Fürste et al., 1986	N/A
p*xcpI*	This Study	N/A
p*xcpJ*	This Study	N/A
p*xcpK*	Bleves et al., 1998	N/A
pKN-ΔH	Durand et al., 2005	N/A
pKN-ΔI	Durand et al., 2005	N/A
Software and algorithms		
NMRPipe	Delaglio et al., 1995	https://www.ibbr.umd.edu/nmrpipe/index.html
NMRFAM-Sparky	Lee et al., 2015	https://nmrfam.wisc.edu/nmrfam-sparky-distribution/
High ambiguity driven protein-protein Docking (HADDOCK)	van Zundert et al., 2016	https://alcazar.science.uu.nl/services/HADDOCK2.2/
Phyre2	Kelley et al., 2015	http://www.sbg.bio.ic.ac.uk/~phyre2/html/page.cgi?id=index
Pymol	Schrödinger and DeLano, 2020	https://pymol.org/2/
Chimera	UCSF	https://www.cgl.ucsf.edu/chimera/
EVcomplex	Hopf et al., 2014	https://v1.evcouplings.org/complex
Spectrum Identification Machine SIM-XL version 1.5.0.14	Lima et al., 2015	http://patternlabforproteomics.org/sim-xl/
Python 3.7.4	Python Software Foundation	https://www.python.org/
Python scripts for filament modeling	This study	https://github.com/EscobarCA/Helix-modeling

(*Continued on next page*)

Please cite this article in press as: Escobar et al., Structural interactions define assembly adapter function of a type II secretion system pseudopilin, Structure (2021), https://doi.org/10.1016/j.str.2021.05.015

Continued

REAGENT or RESOURCE	SOURCE	IDENTIFIER
Other		
Sephacryl S-100 HiPrep 16/60	Cytiva	Cat#17116501
HisTrap FF	Cytiva	Cat# 17525501
HiPrep 26/10 desalting column (Sephadex^{TM} G-25)	Cytiva	Cat# 17508701
ZebaSpinDesalting Column	ThermoFisher	Cat# 89882
Symmetry C18 Trap Column (5 μm, 180 μm x 20 mm)	Waters	Cat# 186007496
HSST3 C18 analytical column (1.8 μm, 75 μm x 250 mm)	Waters	Cat# 186007474

RESOURCE AVAILABILITY

Lead contact

Further information and requests for resources should be directed to and will be fulfilled by the Lead Contact, Katrina T. Forest (forest@bact.wisc.edu).

Materials availability

Protein expression plasmids are available upon request. Strains are available upon request.

Data and code availability

NMR experimental data have been deposited to the BMRB with accession number 50449.

Acidic cross-linking mass spectrometry data are available in the MassIVE database, entries #MSV000086916 and #MSV000086915.

Python scripts used for filament modeling can be found in GitHub (see Key Resources Table for details).

Molecular models have been deposited in the PDB-Dev database (Berman et al., 2019) with accession codes PDBDEV_00000086 for the XcpHIJK quaternary complex and PDBDEV_00000087 for the XcpGHIJK pseudopilus filament.

EXPERIMENTAL MODEL AND SUBJECT DETAILS

Bacterial strains and plasmids

Escherichia coli K-12 DH5α (laboratory collection) and BL21(DE3) pLysS (laboratory collection) were used for cloning procedures and soluble protein production, respectively. *Pseudomonas aeruginosa* PAO1 wild type (laboratory collection), PAO1 *ΔxcpH* (this study), *ΔxcpI* (this study), *ΔxcpJ* (Franz et al., 2011) and *ΔxcpK* (Bleves et al., 1998) or PAO1 *Δxcp* (also called DZQ40) (Ball et al., 1999) strains were used for *in vivo* complementation assays. Construction of the *xcpH* and *xcpI P. aeruginosa* PAO1 deletion strains was performed as described previously (Durand et al., 2005) using the pKN-ΔH and pKN-ΔI mutator plasmids (Table S1). These cells were usually grown at 37°C in LB media. Plasmids used in this study are listed in Table S1. Polymerase Chain Reactions (PCR) were performed using the Q5 high fidelity DNA polymerase (New England BioLabs) for routine cloning or Pfu Turbo (Agilent) for high fidelity and quick-change mutagenesis. Custom oligonucleotides, listed in Table S2, were synthesized by IDT Integrated DNA Technologies (IDT). *P. aeruginosa* chromosomal DNA was used as a template to clone *xcpH* and *xcpH*$_{\Delta 34}$ into the pJN105 backbone using SLIC technology (Jeong et al., 2012) and *xcpI* and *xcpJ* into the pMMB backbone using *Eco*RI restriction site. Site directed mutagenesis was performed using quick change technology or inverse PCR. Plasmid pET-XcpH$_p$ was constructed following the strategy used by Durand et al. (2005) to construct pET-XcpG$_p$. All constructs have been verified by DNA sequencing.

METHOD DETAILS

Gene and protein nomenclature

Here we have extended the general T2SS nomenclature to the *P. aeruginosa* Xcp T2SS components. Thus, former XcpT, U, V, W and X proteins are now labelled XcpG, H, I, J and K in agreement with their homologs in other T2SSs. All pseudopilin soluble domains (deleted for their N-terminal hydrophobic domains (α1N)) used in this study are designated with a subscript p indicating periplasmic. According to the standard in the field, polypeptides are numbered with amino acid 1 as the first residue in the mature pseudopilin following prepilin peptidase cleavage.

LasB secretion and protease activity on plates

Preparation of culture supernatants from *P. aeruginosa* for analysis of secreted proteins has been described (Viarre et al., 2009). Gel analysis was standardized so that the volume of supernatant equivalent to 2 OD_{600} units of culture was used for each sample.

Please cite this article in press as: Escobar et al., Structural interactions define assembly adapter function of a type II secretion system pseudopilin, Structure (2021), https://doi.org/10.1016/j.str.2021.05.015

Protease activity was tested by spotting 5 μl of bacterial culture grown in LB to early stationary phase on TSA plates containing 1.5% lyophilized milk and appropriate antibiotics, followed by 14 h incubation at 30°C.

Protein production and purification

Production and purification of proteins for cysteine cross-linking

Production and purification of $XcpH_p$, $XcpI_p$, $XcpJ_p$, $XcpK_p$, $XcpH_{pV46C}$, $XcpH_{pD49C}$, $XcpH_{pL53C}$, $XcpJ_{pR46C}$ and $XcpJ_{pR53C}$ for cysteine cross-linking (and cross-linking MS experiments was performed in BL21(DE3) pLysS *E. coli* carrying the corresponding pETG-20A plasmid (Table S1) as published (Douzi et al., 2009).

Cell were grown in ZYP-5052 auto induction medium at 37°C until OD_{600} reached 0.8. The cultures were incubated at 17°C for additional 24 hours. Cell were resuspended in Buffer A containing 1 mm EDTA, 0.5 μg/ml lysozyme, phenylmethylsulfonyl fluoride. Cell lysis was performed by a combination of three freeze and thawing cycles and sonication. Lysate was centrifuged at 16,000 x G for 30 min and then dialyzed against 50 mm Tris, 150 mm NaCl, pH 8.0. lysate was loaded to a HisTrap™ FF column, which was washed with Buffer A containing 10 mM imidazole. Elution was performed using Buffer A containing 250 mM imidazole. Imidazole was removed by passing protein sample through a HiPrep 26/10 desalting column (Sephadex™ G-25; Amersham Biosciences). His-tag was cut by incubating protein samples with TEV protease (1mg/mL) for 18 h at 4 °C and removed by passing the sample through a nickel column, untagged protein was collected in the flow-through. Sample buffer was exchanged to 50 mm phosphate, 150 mm NaCl, pH 7 using a Sephadex G75 column.

Production and purification of $XcpH_p$ and $XcpJ_p$ for NMR

Production and purification of $XcpH_p$ and $XcpJ_p$ with or without cysteine substitutions for NMR purposes was carried out with minor modifications from published procedures (Douzi et al., 2009). Expression was performed in BL21(DE3) pLysS *E. coli* carrying the plasmids pETG-20A-$XcpH_p$ or pETG-20A-$XcpJ_p$. For ^{13}C and ^{15}N uniform protein labeling, cells were grown in 3 L of LB at 37°C to OD_{600} ~0.6. Cells were collected and washed with M9 media without glucose or ammonium chloride to remove remaining LB media. After washing, cells were transferred to 1 L M9 media supplemented with 1 g of ^{15}N-U ammonium chloride and 2 g of ^{13}C-U glucose (Cambridge Isotope Laboratories) and incubated at 25°C for 2 hours before inducing with 1 mM IPTG overnight. Purification of $XcpH_p$ proceeded using a combination of nickel affinity and size exclusion chromatography. The cell pellet was resuspended in Buffer A (50 mM tris-HCl buffer pH 8.0 containing 300 mM NaCl) and lysed using a French press. Supernatant from lysate clarified by centrifugation at 25,000 x G for 30 min. was loaded into a 5 mL Ni-NTA column (Quiagen) and washed with 100 mL of Buffer A containing 50 mM imidazole. Protein was eluted from the column using Buffer A with 500 mM imidazole. Peak fractions containing target protein were pooled and treated with TEV protease (purified in house) added to a final concentration of ~40 μg/mL and the sample was dialyzed overnight at 4°C against Buffer A to remove imidazole. Removal of TEV protease proceeded by loading samples into a 1 mL Ni-NTA column which was washed with the same buffer. Fractions containing $XcpH_p$ were collected and concentrated for size exclusion chromatography in a Sephacryl S-100 HiPrep 16/60 column (GE). During this step, buffer was exchanged to NMR buffer (25 mM sodium phosphate buffer pH 6.5 containing 25 mM NaCl). $XcpJ_p$ was expressed and purified using the identical protocol but without ^{13}C and ^{15}N labeling.

Production and purification of $XcpG_p$ and $XcpH_p$ for NMR CSP

Protein purification for NMR experiment shown in Figure S5 was carried out following the procedures published in (Alphonse et al., 2010) for the ^{15}N labelled $XcpG_p$ and in (Durand et al., 2005) for the cold $XcpH_p$ with minor modifications. For ^{15}N-$XcpG_p$ production, BL21 carrying the plasmid pET-$XcpG_p$ was grown in M9 minimal medium supplemented with labeled $^{15}NH_4Cl$ (0.5 g/l). When the OD_{600} of the culture reached 0.6, over-expression was induced with 0.1 mM IPTG and incubation was continued for 13 h. For $XcpH_p$ production, BL21 carrying the plasmid pET-$XcpH_p$ was grown for 4 days in ZYP-5052 auto-inducing medium developed by Studier (Studier, 2014). After growth, the periplasmic fractions containing the soluble recombinant $XcpG_p$ and $XcpH_p$ proteins were obtained from osmotically shocked bacteria and dialyzed overnight at 4°C in dialysis tubing (Sigma) against buffer (50 mM sodium phosphate buffer pH 7, 150 mM NaCl).

In vitro cysteine cross-linking

40 μM of a single cysteine variant or two variant proteins in 1:1 molar ratio were incubated in Tris-HCl 50 mM, NaCl 100mM, pH 8 in a total volume of 500 μL. The mixture was supplemented with DTT (20 mM) to allow reduction of intra-chain disulfide bands formed during purification steps. The mixture was dialyzed against 300 mL of Tris-HCl 50 mM, NaCl 100 mM, pH 8 buffer for 2 h at RT to allow DTT removal and cysteine oxidation. To analyze disulfide bond formation, 75 μL of each reaction was mixed with 25 μL of Leammli loading buffer with or without reductant as appropriate. The samples were heated for 5 min at 95°C and then visualized by 12% Coomassie blue stained SDS-PAGE.

Acidic cross-linking of $XcpH_p$ + $XcpJ_p$ and $XcpH_p$ + $XcpI_p$ + $XcpJ_p$ + $XcpK_p$

Preparation of multimers

For assembling the dimer, 17 μL of $XcpH_p$ at 4 mg/mL were mixed to 25 μL of $XcpJ_p$ at 4 mg/ml, leading to a mixture of 4 nmol of each protein (molar ratio 1:1). For the tetramer, 17 μL of $XcpH_p$ (4 mg/mL), 12 μL of $XcpI_p$ (4 mg/mL), 25 μL of $XcpJ_p$ (4 mg/mL) and 34 μL of $XcpK_p$ (4 mg/mL) were mixed to yield a 4 nmol solution of each protein (molar ratio 1:1:1:1). Samples were dried under vacuum, and dissolved in 100 μL of PBS buffer pH 7.4 to achieve a final concentration of each protein of 40 μM. Proteins were kept at 25°C for 1 h to let the association of the dimer or tetramer occur.

Please cite this article in press as: Escobar et al., Structural interactions define assembly adapter function of a type II secretion system pseudopilin, Structure (2021), https://doi.org/10.1016/j.str.2021.05.015

Cross-linking reaction

To cross-link the dimer, 10 μL of ADH (adipic acid dihydrazide) and 16 μL of DMTMM ((4-(4,6-dimethoxy-1,3,5-triazin-2-yl)-4-methylmorpholinium chloride) were added to the solution of $XcpH_p$:J_p complex, reaching final concentrations of ADH and DMTMM equal to 46 mM (8 and 12.7 mg/mL, respectively). For the tetramer, 23 μL of ADH and 36 μL of DMTMM were added to the solution of $XcpH_p$:I_p:J_p:K_p complex, reaching final concentrations of ADH and DMTMM equal to 81 mM (14.5 and 22.6 mg/mL, respectively). These concentrations were chosen to impose a molar excess of cross-linking reagent of more than 1,000. The mixture was incubated 2 h at 37°C under agitation (750 rpm) to allow intensive cross-linking reaction. The reaction was quenched by reagent removal using a ZebaSpinDesalting Column (0.5 mL, 7k, Pierce), employed according to the manufacturer recommendations. The resulting sample was dried using a Speedvac system.

SDS-PAGE

Cross-linked species were imaged by classical SDS-PAGE analysis. The protein mixture was suspended in 170 μL of 8M urea, leading to a total protein concentration of 48 μM. 20 μg of protein (=10 μL) were dried before being solubilized in 20 μL of Laemmli buffer (Tris HCl pH 6.8 (65 mM), SDS 2%, glycerol 20% and DTT 350 mM) and a spatula tip of bromophenol blue. The sample was heated at 100°C for 5 min, and 10μL (~10 μg) were loaded on the gel (NuPageTM 4-12% Bis-Tris-Gel, 1.0 mm x 10 wells). Migration began with 200 V applied for 40 min (stacking), and then 150 V for the separation. The electrophoresis system was switched-off when the migration blue line reached the extremity of the gel. The gel was fixed 3 h in a bath of 50% ethanol, 47% water and 3% phosphoric acid, washed three times with ultrapure water, and finally incubated in water containing 34% methanol, 17% ammonium sulfate and 3% phosphoric acid. Coloration of bands was accomplished over 3 days with Coomassie blue G250 added at 360 mg/l in the solution. The gel was finally washed several times in pure water to remove the excess of Coomassie blue.

In-gel digestion

The bands corresponding to the $XcpH_p$:$XcpJ_p$ dimer or $XcpH_p$:$XcpI_p$:$XcpJ_p$:$XcpK_p$ tetramer, respectively, were excised, and cut into small pieces. Resulting pieces of gel were then washed by 50 μL of 50 mM NH_4HCO_3 then centrifuged (5 min, 600 rpm) to remove the supernatant. The same step was repeated with 50μL of 50/50 (v/v) 50 mM NH_4HCO_3/acetonitrile. The two previous steps were repeated twice. To ensure a good penetration of the enzymes into the pieces of gel, the latter were dehydrated twice with 50 μL of pure acetonitrile removed by centrifugation (5 min, 600 rpm). The gel was then rehydrated at 0°C with 3μL of a solution containing 1/100 of Lys-C and 1/50 of trypsin in 50 mM NH_4HCO_3. The digestion was performed at 37°C for 4 hr. Enzymatic activity was quenched by acidifying the medium using 25 μL of 1% trifluroroacetic acid. Resulting peptides were eluted from the gel by incubating the sample overnight at 20°C under 600 rpm.

LC-MS/MS

1 μg of the digested material was analysed using a UPLC nanoACQUITY (Waters, UK) coupled to a Q-Exactive Plus Hybrid Quadrupole-Orbitrap Mass Spectrometer (Thermo Scientific, USA). The chromatographic system is equipped with two columns. The first one, dedicated to the trapping of peptides, is a Symmetry C18 (5 μm, 180 μm x 20 mm, Waters, UK). The second one which performs the analytical separation is a HSST3 C18 (1.8 μm, 75 μm x 250 mm, Waters). The dimensions given for the columns are in the order: particle diameters, internal diameters and column lengths. Solvent A was water, acidified with 0.1% formic acid and solvent B was acetonitrile, also acidified with 0.1% formic acid. Cross-linked peptides were first trapped for 3min (98/2, v/v, A/B) at a flow rate of 20μL/min before being eluted with a gradient of 57 min at a flow rate of 700 nL/min. The elution started with a linear gradient of B from 2% to 7% in 5 min, followed by an increase from 7% to 40% in 25 min, then to 85% in 3 min. This composition A/B 15/85 is kept for 5 min before changing to 98/2 for reconditioning the analytical column. The Q-Exactive Plus spectrometer was set in a nanoESI positive mode acquisition for 57 min. The acquisition was recorded in full scan MS and data dependent MS/MS, in a mass range m/z 400-1,750. For the MS stage, resolving power was set at 70,000 @m/z 200, with an automatic gain control (AGC) target at 1e6 (or 50 ms as a maximum injection time). For MS/MS, a "Top 12" experiment was applied, meaning that the twelve most intense ions of each MS scan were selected for fragmentation. Singly charged ions, ions with undetermined charge (for example, electronic noise) and ions with signal intensities below the AGC threshold set at 1e3 were excluded from this selection. For precursor ions, the selection window was 2.0 m/z, the AGC target was 1e5 (or 50 ms as a maximum injection time) and the resolving power of 17,500 @m/z 200. Normalized collision energy was 25. A dynamic exclusion of 10s was also applied to avoid the redundancy of MS/MS spectra of the same ions.

NMR experiments

All solution NMR experiments (except $XcpH_p$/G_p chemical shift perturbation) were run at 37°C in a Bruker 900 MHz NMR spectrometer at the National Magnetic Resonance Facility at Madison. Sample condition used was NMR buffer containing 0.01% sodium azide, 50 μM 2,2-dimethyl-2-silapentane-5-sulfonate (DSS) (Sigma) and 8% D_2O.

$XcpH_p$ NMR assignments

Backbone sequential assignments were carried out using standard 3D NMR experiments including HNCO, HN(CA)CO, HNCACB, CACB(CO)NH. These experiments were collected using non-uniform sampling (NUS). Data processing of NUS data was performed using NMRPipe (Delaglio et al., 1995). Chemical shift referencing was done using DSS as reference. Backbone assignments were facilitated using NMRFAM-Sparky software (Lee et al., 2015). Calculation of secondary chemical shifts for secondary structure estimation was done using random coil chemical shifts calculated for the XcpH amino acid sequence using ncIDP library (Tamiola et al., 2010). Secondary chemical shifts were calculated as $\Delta\delta Ca - \Delta\delta Cb$, where $\Delta\delta Ca = (\delta Ca_{XcpH} - \delta Ca_{random\ coil})$ and $\Delta\delta Cb = (\delta Cb_{XcpH} - \delta Cb_{random\ coil})$. This step effectively removes any error in chemical shift referencing.

Please cite this article in press as: Escobar et al., Structural interactions define assembly adapter function of a type II secretion system pseudopilin, Structure (2021), https://doi.org/10.1016/j.str.2021.05.015

$XcpH_p$ and $XcpJ_p$ chemical shift perturbation assays

Chemical shift perturbation assays were carried out using 100 μM ^{15}N-U XcpH and increasing amounts of unlabeled XcpJ (20 μM, 50 μM, and 80 μM). An independent ^{1}H-^{15}N HSQC spectrum was collected for each sample. Total change of the amide proton and nitrogen chemical shift (ΔδNH) was calculated for each residue as $((\Delta\delta H)^2 - 1/6\ (\Delta\delta N)^2)^{1/2}$, were ΔδH and ΔδN correspond to the difference in chemical shift of proton and nitrogen respectively. ΔδNH was calculated using the control spectrum as the initial point and the spectrum with 80 μM XcpJ as the endpoint.

$XcpH_p$ and $XcpJ_p$ paramagnetic relaxation enhancement assay

To perform paramagnetic relaxation enhancement (PRE) experiments, four different $XcpJ_p$ cysteine mutant constructs (R46C, R53C, T178C, E180C) were used to attach the spin label (1-Oxyl-2,2,5,5-tetramethylpyrroline-3-methyl) methanethiosulfonate (MTSL) (Santa Cruz Biotechnology). $XcpJ_p$ variants were purified as above in Buffer A containing 1 mM DTT. MTSL labeling of $XcpJ_p$ was performed in NMR buffer and 0.5 mM DTT. $XcpJ_p$ samples were incubated with a 20x molar excess of MTSL for 4 h at room temperature. Additional 20x molar excess of MTSL was added to the sample which was further incubated at room temperature overnight. Excess MTSL was removed by dialysis against the NMR buffer. The NMR sample contained 80 μM ^{15}N-U $XcpH_p$ and 24 μM of MTSL labeled $XcpJ_p$. The ratio of XcpH to $XcpJ_p$ was selected based on the chemical shift perturbation assay to avoid signal loss due to complex formation. A 2D ^{1}H-^{15}N HSQC spectrum was acquired for each sample. After collecting the HSQC experiment of the oxidized or paramagnetic form of MTSL, 2 mM sodium ascorbate (Sigma-Aldrich) was added to the sample and incubated at room temperature for at least one hour before collecting the spectrum of the reduced or diamagnetic MTSL form. Effects of the paramagnetic label were quantified as the ratio of signal intensity of the spectrum collected with MTSL in paramagnetic versus diamagnetic form (I_{para}/I_{dia}).

$XcpG_p$ and $XcpH_p$ chemical shift perturbation

2D ^{1}H-^{15}N HSQC spectra were collected for 120 μM ^{15}N $XcpG_p$ alone or in the presence of unlabeled $XcpH_p$ at 480 μM in 25 mM sodium phosphate buffer pH 6.5 containing 125 mM NaCl and 8% D_2O. Independent 2D ^{1}H-^{15}N HSQC spectrum was collected for each sample in a Bruker Avance III 600MHz NMR spectrophotometer.

Quaternary complex computational modeling

Modeling of the $XcpH_pI_pJ_pK_p$ quaternary complex was achieved using high ambiguity driven protein-protein Docking (HADDOCK) (van Zundert et al., 2016). Structures used for HADDOCK corresponded to the $XcpI_pJ_pK_p$ crystal structure (PDB: 5VTM) and an $XcpH_p$ model prepared based on the structure of $EpsH_p$ from *Vibrio cholerae* (PDB: 2QV8) using the Phyre2 server (Kelley et al., 2015). Allowed distances for acidic cross-linking restraints between C_α carbons were set between 8-18 Å, while 6-18 Å were used for PRE restraints (Tables S3 and S4). Docking the $XcpH_p$ model onto the $XcpI_pJ_pK_p$ structure was performed using the HADDOCK 2.2 server (van Zundert et al., 2016). The highest scoring structure obtained from HADDOCK which also did not have perpendicular α1C helices in the pseudopilins was selected for further analysis of the $XcpH_pI_pJ_pK_p$ complex.

Biological filament modeling

Modeling of the XcpG T2SS pseudopilus was based on the PulG filament structure from *Klebsiella oxytoca* (Lopez-Castilla et al., 2017) (PDB: 5WDA) using PyMOL (Schrödinger and DeLano, 2020). Modeling was divided in the following steps: (1) adding missing transmembrane helices to each of the five $XcpG_p$, $XpcH_p$, $XcpI_p$, $XpcJ_p$, and $XcpK_p$ proteins, (2) positioning the XcpHIJK complex onto the PulG electron microscopy reconstruction filament (3) fitting XcpHIJK helices to the positions of PulG transmembrane helices within this filament (4) fitting XcpG (Alphonse et al., 2010) units to the PulG filament and (5) relaxing the whole system to remove atomic clashes. Each of these steps is described in more detail below.

Modeling of missing transmembrane helices

Missing transmembrane helices in minor and major pseudopilins were initially predicted using the Phyre2 server inputting the respective amino acid sequence of the complete N-terminal alpha helix (α1N + α1C). The XcpG helix was modeled based on the PulG template from the EM reconstruction to include the unraveled section. The XcpHIJK helices were initially based on 1OQW template, as chosen by Phyre2. Subsequently, the XcpH helix was also modeled based on the PulG template from the EM reconstruction to include the unraveled section.

The following steps were performed in PyMOL. To position the modeled α1 helices, each was computationally aligned to the respective α1C in the HADDOCK model or the $XcpG_p$ solution NMR structure (PDB: 2KEP) (Alphonse et al., 2010). Special care was taken to manually reposition if needed so that the C-terminal atom in the missing α1N region was within covalent bonding distance from the N-terminal atom in the soluble construct α1C helix. Then, atoms in the modeled helices belonging to the α1C sequence were deleted. Finally, the modeled helices were added to the $XcpH_pI_pJ_pK_p$ complex and $XcpG_p$ PDB files. At this stage, the transmembrane helices were not in a biologically relevant conformation, which was addressed at a later stage (see below, "Modeling of transmembrane helix positions").

Positioning the XcpHIJK complex onto the PulG filament

In PyMOL, the XcpHIJK complex with its full-length helices was positioned onto the PulG filament by aligning the XcpH soluble domain with the fourth PulG unit soluble domain. The positioning of XcpH to the fourth PulG unit (counted from the tip), rather than the first, was decided to allow PulG units 1 to 3 to serve as reference for the modeling of XcpIJK transmembrane helices. During this phase, globular domains of XcpH, XcpI, and XcpK were fixed and no attention was paid to how they mapped onto PulG globular domains.

Please cite this article in press as: Escobar et al., Structural interactions define assembly adapter function of a type II secretion system pseudopilin, Structure (2021), https://doi.org/10.1016/j.str.2021.05.015

Modeling of transmembrane helix positions

XcpHIJK model transmembrane helices were modeled semi-manually to fit the interior cavity of the PulG filament. To guide the modeling, the transmembrane helix of the PulG unit closest to a given minor pseudopilin was used as a reference. Thus, PulG units 1, 2, 3 and 4 were the reference for XcpK, XcpI, XcpJ and XcpH respectively. The goal of this stage was a coarse arrangement of subunit helices. We expected the subsequent relaxation step (described below) would further address helix packing, improve geometry and enforce the F1-E5 salt bridge. Custom Python scripts were used to modify Φ and Ψ dihedral angles for some residues in the transmembrane helices. Φ and Ψ dihedral angles were systematically varied to each of 39 Φ/Ψ pair values observed in α1 residues in the XcpH Phyre2 model structure; these smoothly populated the a helical region of the Ramachandran plot from Φ = -38.4 to -116.4 and Ψ = -11.1 to 81.4.

The general modeling process proceeded as follows. First, residues ranges for optimization were chosen by simple manual inspection of where along α1 slight deviations in its trajectory would be likely to bring it into closer alignment with the PulG reference helix for that subunit. Secondly, for each of these *n* residues, one at a time iteratively starting nearest the C-terminus, the Φ and Ψ angles were exchanged for the new Φ/Ψ pair value from the list, generating 39 new structures at each step. The script outputs a pdb file with each model included as a state, which can be viewed as a movie in PyMOL (see movie for example in GitHub link in key resources table). At each step, these 39 models were ranked within the Python script to favor the smallest distance from the N-terminal residue Cα of the modified helix to the PulG reference N-terminal residue Cα in order to promote favorable close packing of helices in the filament. In addition, caution was taken to avoid significant clashes with other helices, this was evaluated by simple observation of the models. A model was selected and used as input for the same modification process at the next residue, thus iterated *n* times. The logic for the order of residues to which the algorithm was applied was that Φ/Ψ angles closer to the C-terminus would have significant impact on the helix trajectory, followed by residues closer to the N-terminus for fine modification. Thus in total n*39 new models were evaluated. This entire procedure was repeated until it converged with a close match between the modified and reference PulG helices.

After modeling was completed, the presence of the N-term to E5 salt bridge was evaluated. XcpI and XcpJ distances were 4.6 Å and not further modified. For XcpX, the N-terminus of the PulG subunit 1 reference helix itself was in a clashing position and therefore the above procedure could not lead to a satisfactory outcome. Thus, additional iterations were performed on XcpX residues 1-5 using the N-term to E5 salt bridge as a ranking measure.

XcpH was a special case for which early on in the procedure it was clear no satisfactory solution would be achieved using the initial XcpH helix model derived from 1OQW. Using the subsequent unraveled model, only residues 1 to 18 were modified in the procedure described above, so as not to impact the unraveled region which was already a fairly good match to PulG. In this case, the N-term to E5 salt bridge was used for the output ranking for all iterations.

Modeling of XcpG filament

To model the XcpG pseudopilus, PulG subunits were simply replaced with XcpG to complete the filament. In PyMOL, the modeled XcpG unit was copied and aligned to each PulG unit. Finally, all PulG units (including the reference) were removed and the final XcpG filament was saved as a new object.

Relaxing the Xcp pseudopilus

Ultimately, the complete filament model was relaxed with pyRosetta (Chaudhury et al., 2010). During this procedure, the known salt bridge between E5 carboxyl group and N-terminal amino group of the next subunit in the filament was enforced as a distance restraint of 2.8 Å. Other restraints were added from the Haddock quaternary model protein:protein interactions to maintain the quaternary tip complex structure (~10 for each pseudopilin pair for a total of 53 restraints ranging from 5.3-28.2 Å) and from the XcpG filament (10 total ranging from 2.8 – 21.5 Å). Restraints are listed in Tables S5 and S6. Ten filament models were produced, from which the best was selected based on favourable XcpG subunit packing and the lowest RMSD of the $XcpH_pI_pJ_pK_p$ tip structure with respect the HADDOCK model.

Positioning of the pseudopilus into secretin and T2SS maps

The pseudopilus model generated in this study was manually fitted into the XcpD EM map (EMD 8820) using Chimera. Fitting of the pseudopilus-secretin model into the ETC maps of the *L. pneumophila* T2SS was carried out following these steps: the model of pseudopilus-secretin built and presented in panel (a) was superimposed on the subtomogram average based on the position of the secretin gate by using the ECT map of the *L. pneumophila* (EMD 20713). The resulting model was superimposed on the subtomogram average of the ECT map of *L. pneumophila* (EMD 20712) based on the OM position. Both images were made using Chimera.

Evolutionarily coupled residues between $XcpH_p$ and $XcpJ_p$

The amino acid sequences of $XcpH_p$ and $XcpJ_p$ were analysed using the EVcomplex submission tool of the "EVolutionary Couplings" webserver with default parameters (Hopf et al., 2014) (https://v1.evcouplings.org/complex). 2052 homolog sequences were identified and aligned with a quality ratio of 3.01, considered "good" by the program. Based on amino acid conservation in all aligned sequences, the program generated a set of residues that are evolutionarily coupled. Only residue pairs with a probability score greater than 0.92 were included in the subsequent analysis. Analysis is represented on a graph where X and Y axes correspond to input sequences (the 144 residues of $XcpH_p$ followed by the 210 residues of $XcpJ_p$) whereas, evolutionarily-coupled residues between $XcpH_p$ and $XcpJ_p$ are indicated by grey dots circled following a color code at the position corresponding to $XcpH_p$ and $XcpJ_p$ sequence coordinates. The identified EV-coupled residues have been highlighted on the 3D structure of the quaternary complex following the color code used on the graph.

Please cite this article in press as: Escobar et al., Structural interactions define assembly adapter function of a type II secretion system pseudopilin, Structure (2021), https://doi.org/10.1016/j.str.2021.05.015

QUANTIFICATION AND STATISTICAL ANALYSIS

Cross-linking data analysis

Spectrum Identification Machine SIM-XL version 1.5.0.14 (Lima et al., 2015) was used for identification of cross-linked peptides. ADH-DMTMM cross-linker was set up in the software to create a mass shift of 138.0905 Da for each cross-link and 156.1012 for hydrolyzed monolinks. The possible reaction sites were restricted to C-terminal extremities and acidic side chains of Glu and Asp amino acids. Accuracy on mass measurements was 2 ppm for the precursor and 10 ppm for the fragment ions, to reduce to their maximum the false positives and to increase the reliability of the results. Oxidation of methionine, due to experimental conditions, has also been considered as a variable modification. Only the cross-linked peptides characterized by a SIM-XL internal score of 2.5, 3.0, 2.3, 3.0 or 2.5 and higher have been retained for XcpIK, IJ, HJ, HI, or HK pairs, respectively. All the detected cross-linked peptides have been manually validated by analyzing their corresponding MS/MS spectra for exact masses, numbers of identified fragments, and signal intensity (*e.g.* Figures 6B and S3B).